How conspicuous are peacock eyespots and other colorful feathers in the eyes of mammalian predators?

3   Suzanne Amador Kane[1*], Yuchao Wang[1], Rui Fang[1] , Yabin Lu[1] , Roslyn Dakin[2]

4   [1] Physics & Astronomy Department, Haverford College, Haverford, PA, USA

5   [2] Migratory Bird Center, Smithsonian Conservation Biology Institute, National Zoological Park,

6   Washington, DC, USA

7

8   *corresponding author

9   Email: samador@haverford.edu

10

11   **Short title:** Are colorful feathers conspicuous in the eyes of mammalian predators?

12

13   **Keywords: color vision, predation, feather, multispectral imaging, camouflage, distance**

14

Abstract

16   Feathers perceived by humans to be vividly colorful are often presumed to be equally

17   conspicuous to other mammals, and thus to present an enhanced predation risk. However, many

18   mammals that prey on adult birds have dichromatic visual systems with only two types of color-

19   sensitive visual receptors (one sensitive to ultraviolet light), rather than the three characteristic of

20   humans and four of most birds. Thus, understanding how these predators perceive color requires

21   quantitative visual modeling. Here, we use a combination of reflectance spectroscopy,

22   multispectral imaging, color vision modelling and visual texture analysis to compare the visual

23   signals available to conspecifics and to mammalian predators for multicolored feathers from the

24   Indian peacock (*Pavo cristatus*) as well as red and yellow parrot feathers; we also take into

25   account the effects of distance-dependent blurring due to visual acuity. When viewed by

26   tetrachromatic birds against a background of green vegetation, most of the feathers studied had

27   color and brightness contrasts similar to values previously found for ripe fruit. By contrast,

28   when viewed by dichromat mammalian predators, the color and brightness contrasts of these

29   feathers were only weakly detectable and often did not reach detection thresholds for typical

30   viewing distances. We furthermore show that the peacock's erect train has undetectable color

31   and brightness contrasts and visual textures when photographed against various foliage

32   backgrounds. Given the similarity of photoreceptor sensitivities and feather reflectance

33   properties across relevant species, these findings are consistent with many feathers of similar hue

34   being inconspicuous, and in some cases potentially cryptic, in the eyes of their mammalian

35   predators. These results suggest that many types of colorful feathers are likely to be cryptic to

36   mammals while providing a communication channel perceptible to birds, while emphasizing the

37   importance of understanding diverse sensory receivers in the evolution of animal coloration.

38

Introduction

40   Ever since Darwin, colorful feathers such as the iridescent eyespots of the Indian peacock (*Pavo*

41   *cristatus*) (Fig 1A) have been assumed to present salient visual signals readily detectable by their

42   natural predators (Darwin, 1888; Ranjith and Jose, 2016; Ruxton et al., 2004). For this reason,

43   these sexually-selected ornaments have been proposed to incur a cost due to increased predation.

44   For example, as Zahavi stated in his paper introducing the handicap principle: "The more

45   brilliant the plumes, the more conspicuous the male to predators" (Zahavi, 1975). Evidence for

46   such countervailing selection pressures has been found in ornamented guppies preyed upon by

47   fish (Endler, 1980) and in birds preyed upon by other birds (Møller and Nielsen, 2006).

48   However, while this assumption is predicated on the predator being able to detect prey visual

49   signals (Outomuro et al., 2017), no studies have tested whether this is true for the mammalian

50   predators that prey on many birds. For example, the primary predators of adult peafowl are

51   carnivorans (felids and canids, S1 Appendix), which all have dichromatic visual systems; i.e.,

52   they have only two types of cone visual receptors with distinct spectral sensitivities, not the four

53   characteristic of most birds (Cronin et al., 2014) or the three found in most humans. More

54   generally, felids (e.g., *Felis catus*) are a major threat to bird populations world-wide (Loss et al.,

55   2015). Because dichromatic mammals lack red-green color discrimination, they are unlikely to

56   detect many of the chromatic visual cues evident to birds and humans (Cronin et al., 2014; Miller

57   and Murphy, 1995). Studies of visual ecology have considered how prey appear to various types

58   of predators (birds, insects and fish) for many types of prey, including insects and birds (Håstad

59   et al., 2005; Théry et al., 2005), fish (Endler, 1991), cuttlefish (Chiao et al., 2011), crustaceans

60   (Nokelainen et al., 2017), primates (Sumner and Mollon, 2003) and lizards (Outomuro et al.,

61   2017). Two previous studies also have studied the iridescence reflectance spectra of peacock

62   eyespots and how they are perceived by peahens (females) (Dakin and Montgomerie, 2013;

63   Loyau et al., 2007). As yet, no studies have compared how visual signals from peacocks and

64   other avian prey appear in the vision of their mammalian predators.

65

66   **Fig 1. Peacocks and the model peacock train.** A) An Indian peacock displaying his erect train

67   to a peahen (female) in the foreground and B) another individual holding his train folded while

68 walking. C) Model peacock train assembled from a collection of eyespot feathers used to

69 evaluate the appearance of the train viewed against vegetation.

70

71

72 During courtship displays, male Indian peafowl ("peacocks") attract mates by spreading, erecting

73 and vibrating the fan-like train ornament (Fig. 1A), causing it to shimmer iridescently and emit

74 mechanical sound (Dakin and Montgomerie, 2009; Dakin et al., 2016; Freeman and Hare, 2015).

75 Several lines of evidence indicate that these feathers are assessed during mate choice: train-

76 rattling performance by peacocks is obligatory for mating success (Dakin and Montgomerie,

77 2009), eye-tracking experiments have shown that train-rattling displays are effective at attracting

78 and holding the peahen's gaze (Yorzinski et al., 2013), and eyespot iridescence has been shown

79 to account for approximately half of variation in male mating success (Dakin and Montgomerie,

80 2013; Loyau et al., 2007). Because peacocks spend the majority of their time in activities other

81 than courtship displays even during the breeding season (Dakin and Montgomerie, 2009;

82 Harikrishnan et al., 2010), any test of visual saliency must also consider the appearance of the

83 folded train. Furthermore, because the peacock's head, neck and breast are covered by iridescent

84 blue contour feathers (Yoshioka and Kinoshita, 2002), the visual cues generated by this body

85 plumage are also relevant for salience to potential mates and predators.

86

87 Here, we use multispectral imaging and reflectance spectroscopy to compare how detectable

88 peacock feathers are to conspecifics and dichromatic mammalian predators (hereafter

89 "dichromatic mammals"), as measured by color, brightness, and texture contrast relative to green

90 background vegetation, following similar studies of prey that utilize camouflage against

91   predators with a variety of visual systems (Stevens and Merilaita, 2011). Our goal was to test the

92   assumption that colorful feathers that are highly conspicuous to conspecific birds are also readily

93   detectable by these predators. To determine how generalizable our results were to other hues of

94   colorful plumage, we also measured reflectance spectra and multispectral images of red and

95   yellow parrot feathers. We then used psychophysical vision models to test whether conspecifics

96   and dichromatic mammalian predators can readily detect the color and brightness contrasts

97   between feathers and green vegetation. Our analysis modeled the appearance of feathers at

98   various distances to determine when each observing species could distinguish color patches

99   relative to the surrounding environment.

100

101   In addition to color cues, visual salience depends on the presence of pattern features that are

102   perceptually discriminable from the background. To determine whether predators might detect

103   the peacock's train using such visual texture cues, we analyzed images of the model train relative

104   to that of background vegetation using two pattern analysis methods motivated by visual

105   processing in vertebrates (Stoddard and Stevens, 2010). Granularity analysis is a spatial filtering

106   method that determines the contributions to image contrast of features with different sizes; this

107   image processing technique has been used to compare pattern textures in studies of cephalopod,

108   avian egg, fish and shore crab camouflage, as well as humans searching for objects against

109   various backgrounds (Akkaynak et al., 2017; Barbosa et al., 2008; Nokelainen et al., 2017;

110   Stoddard and Stevens, 2010; Troscianko et al., 2017). A second method, edge detection,

111   provides a complementary measure of texture complexity by using image processing to detect

112   sharp gradients in intensity (Stoddard et al., 2016).

113

Materials and methods

Feather samples

Five Indian peafowl eyespot (Fig 2A), three blue peacock contour breast feathers (Fig 2B), four

scarlet macaw (*Ara macao*) wing feathers (two red and six yellow patches total) (Fig 3A), two

Amazon parrot wing feathers (two red and two yellow patches total) (Fig 3B), and four red

African grey parrot (*Psittacus erithacus*) tail feathers (Fig 3C) were obtained from Moonlight

Feather (Ventura, CA USA) and Siskiyou Aviary (Ashland, OR USA). Because the

psittacofulvin pigments in parrot feathers have reflectance spectra with similar spectral features

to red and yellow carotenoid pigments (Shawkey and Hill, 2005; Toral et al., 2008), our results

should be representative of red and yellow feathers in general. Our number of replicates for the

peacock eyespots agree well with recommendations from a study of intraspecies variations in

feather color measures (Dalrymple et al., 2015); however, we were limited by availability to

fewer replicates for the parrot feathers. For mounting, eyespot feathers were cut off below the

outermost colored ring at the proximal end. All feather types were mounted on black matte art

quality paper with a magnetic backing that adhered to the tilt stages used for spectroscopy and

multispectral imaging. Feather samples were stored without compression in sealed boxes in

acid-free envelopes at 75% relative humidity and ambient temperature (22 ± 2 deg C). The

different peacock eyespot color patches (colored rings and central disk) are referred to using the

names and two letter abbreviations indicated in Fig 2A.

Fig 2. Peafowl cone sensitivity spectra and peacock feather vs green vegetation reflectance

spectra. (A) An Indian peacock eyespot feather showing the color patch names used in the

analysis. (B) Peacock blue breast plumage. (C) Comparison of the cone photoreceptor spectral

137   sensitivities for the Indian peafowl and ferret, which has dichromatic color vision very similar to

138   that of cats and dogs. All spectra are multiplied by the D65 illuminance spectrum used to model

139   sunlight and normalized to unit area. Reflectance spectra of (D) peacock feather eyespots and

140   (E) peacock iridescent blue body plumage and the green saucer magnolia (*Magnolia x*

141   *soulangeana*) leaf used as a background for the feather sample images.

142

143   **Fig 3. Parrot feather images, cone sensitivity spectra and feather reflectance spectra.** (A)

144   Scarlet macaw, (B) Amazonian parrot and (C) African grey parrot feather samples. (D)

145   Comparison of the cone photoreceptor spectral sensitivities for the blue tit, which has

146   tetrachromatic ultraviolet sensitive (UVS) color vision similar to that of parrots, and the ferret,

147   which has dichromatic color vision similar to that of cats and dogs. All spectra are multiplied by

148   the D65 illuminance spectrum used to model sunlight and normalized to unit area. (E)

149   Reflectance spectra of the parrot feather red and yellow patches studied here.

150

151   We also assembled an array of 28 peacock feathers (Fig 1C) to create a model train arranged to

152   match the geometry of eyespots in actual peacock trains ((Dakin and Montgomerie, 2013)); this

153   was used to simulate the appearance of the train during display (when the train is erect) or during

154   walking, perching or standing (when the train is held horizontally; see Fig 1B). In their native

155   range in India and Pakistan, peafowl are reported to live in a variety of habitats, including open

156   moist and dry-deciduous forest, scrub jungle, and adjacent grasslands, and their breeding season

157   is reported to coincide with the start of the rainy season (Gokula, 2015), after which eyespot

158   feathers are shed by molting (Beebe, 1918; Sharma, 1974). We used as background foliage for

159   feather and model train images various plants (grass, brush and trees) native to the northeast

160   USA (S2 Appendix). Because green flora have generic reflection spectra due to chlorophyll

161   absorption (Jensen, 2009), the plants used in this study should be representative of the color and

162   luminance of those found in the native environments of peafowl and many other bird species.

163

Vision models

164

165   The Indian peafowl's visual system has four classes of color-sensitive (chromatic) single cone

166   cells: violet (VS), short (SWS), medium (MWS) and long (LWS) wavelength-sensitive cones,

167   and one type of double cone that is sensitive to brightness (luminance) (Hart, 2002). In order to

168   illustrate their spectral responses under natural illumination, Fig 2C shows the peafowl cone's

169   spectral sensitivities $S_r(\lambda)$ for the rth photoreceptor type (including ocular media and oil droplet

170   transmission) multiplied by the CIE D65 irradiance spectrum, $I(\lambda)$, and normalized to unit area;

171   we used this standard illuminant because of its close match the solar irradiance spectrum for the

172   elevation angles found for actual peacock displays (Dakin and Montgomerie, 2009; Spitschan et

173   al., 2016). To model the tetrachromatic UVS (ultraviolet-sensitive) vision of parrots we used

174   blue tit (*Cyanistes caeruleus*) cone spectral sensitivities (Hart et al., 2000; Troscianko and

175   Stevens, 2015). (Fig 3D).

176

177   The visual systems of dichromatic mammalian predators have been studied for a variety of

178   genera, and found to include S (blue- to near-UV-sensitive) (Douglas and Jeffery, 2014) and L

179   (green-sensitive) cone populations in all carnivorans studied to date, including felids (Guenther

180   and Zrenner, 1993) and canids (Jacobs et al., 1993). Behavioral studies have confirmed that

181   domestic cats (Clark and Clark, 2016) and dogs (Kasparson et al., 2013; Neitz et al., 1989) have

182   dichromatic color vision. Brightness signals in dichromatic mammals are assumed to be due to

183 only the L cones (Osorio and Vorobyev, 2005). We used ferret (*Mustela putorius*) cone spectra

184 (Troscianko and Stevens, 2015) to model dichromat vision because ferret spectral peaks agree

185 closely with those of cats and dogs (i.e., $\leq 4.4\%$ for S and $\leq 1.4\%$ for L cones) (Calderone and

186 Jacobs, 2003; Guenther and Zrenner, 1993; Jacobs et al., 1993) (Fig 2C). While many

187 carnivorans are primarily nocturnal or crepuscular, at low light levels, photopic chromatic signals

188 will be weak and visual signals will be dominated by luminance contrast via rods or double

189 cones. Thus, we consider high luminance photopic conditions as the best case scenario for visual

190 detection by these predators.

191

Multispectral imaging

193 Multispectral images were recorded using a GoPro Hero 4 Silver Edition camcorder (GoPro Inc,

194 San Mateo, CA USA) modified for full spectral imaging by replacing its original lens and

195 infrared (IR) filter with a quartz lens transparent to < 300 nm (Igoe et al., 2013; Prutchi, 2016).

196 Because the spectral response of this camera's IMX117 Exmor-R CMOS sensor (Sony Corp.,

197 Tokyo, Japan) is sensitive throughout the visible and near-UV, these cameras have been used in

198 multispectral imaging (Vogt and Vogt, 2016; Yun et al., 2016) (S1 Fig). Multispectral

199 photographs were recorded at 3000 × 2250 pixel resolution and the GoPro settings medium field

200 of view, Protune CAM-RAW mode (for no white balance compensation), flat color, low

201 sharpness, ISO 400, exposure -2, night mode (to enable shutter speed control), auto shutter and

202 spot meter on. Each sample was photographed for each geometry and illumination condition to

203 give two multispectral images: 1) a UV image using an Andrea-UV filter (< 1% transmission for

204 > 400 nm; UVIROptics, Eugene, Oregon USA; 2) a visible RGB (red, green, blue) image using

205 two UV-IR cut filters to pass 400-700 nm light (Hoya Corp., Tokyo Japan). Filter transmission

206   spectra were measured using the methods described below in "Reflectance Spectroscopy" (S1

207   Fig). The camera's large depth-of-field eliminated the need for refocusing between visible and

208   UV images. To maintain constant camera alignment between photographs, we mounted the

209   camera rigidly using optical mounts (Thorlabs, Newton NJ, USA) and attached filters using

210   quick-release Xume magnetic adapters (Panalpina Inc., Port Reading, NJ, USA); all images were

211   taken using a remote trigger. Each feather image included a model Micro FSS08 8-step

212   grayscale diffuse reflectance standard (Avian Technologies, New London, NH USA) mounted

213   level with the sample plane for calibrating absolute reflectance (Troscianko and Stevens, 2015).

214   Images of the model train included a larger 6-step grayscale and color checker chart (DGK Color

215   Tools WDKK Waterproof, Digital Image Flow, Boston MA USA). Reflectance spectra for each

216   grayscale in each filter and camera color channel combination were measured using the methods

217   described below in "Reflectance Spectroscopy". Each image also included an object of known

218   size for spatial calibration.

219

220   All samples were mounted on a tripod for imaging (S2 Fig). Three sets of multispectral images

221   each were obtained with the model train held erect and held horizontal viewed from the side.

222   Peacock eyespots were oriented with their rachis vertical to simulate their average orientation in

223   the erect train during courtship displays and the model train was oriented in a variety of

224   directions to simulate the variation in appearance of the iridescent train eyespot feathers during

225   courtship display, standing and walking. The camera was mounted on a second tripod a distance

226   20.0 ± 1.0 cm from feather samples and 1.70 to 2.00 ± 0.05 m from the model train. For feather

227   samples, the camera was oriented to record images at normal observation angle ($\theta = 0 \pm 2$ deg)

228   with respect to the feather sample plane (Fig 4). The size of feather sample images was 55 mm x

11

229   67 mm, corresponding to 7.3 pixel/mm. Images were captured during June-July 2018 in the

230   Haverford College Arboretum (latitude, longitude: 40.0093° N, 75.3057° W) for 24.2 ± 0.2 deg

231   C and 55.5 ± 1.5 % relative humidity. All feather samples were illuminated by direct sunlight

232   with an azimuthal angle $\Psi = 45 \pm 3$ deg clockwise from the camera's optical axis and at solar

233   elevation angles $\Phi = 30 \pm 3$ deg, corresponding to an angle $\alpha = 52 \pm 3$ deg between the

234   observation and illumination directions (Fig 4). These illumination and observation angles agree

235   with those measured for female peafowl observing courtship displays (Dakin and Montgomerie,

236   2009). In general, these solar angles hold for the early morning times when most birds are most

237   active (Robbins, 1981). Optimal color contrasts for non-iridescent feathers have been found to

238   correspond to the range of observation-illumination angles α used in this study (Barreira et al.,

239   2016); this is relevant because pigment-based colors can appear in combination with structural

240   coloration (Shawkey and Hill, 2005). Furthermore, for this observation geometry, the bird's

241   body subtends the greatest visual angle. The peacock eyespot feather samples were surrounded

242   by additional loose green barbs to simulate their setting in the actual train, while the parrot

243   feather samples were surrounded by a saucer magnolia leaves picked ≤ 1 hour before image

244   capture. We also imaged a variety of green leaves for comparison (S3 Fig). Black velvet fabric

245   was mounted behind the feather samples to limit backscattered light and a lens hood was used to

246   reduce lens flare. The model peacock train was photographed against a variety of foliage

247   backgrounds for solar elevation angle between 37 to 55 deg.

248

249   **Fig 4. Multispectral imaging geometry showing the angles of observation and illumination**.

250

251   Multispectral images were first processed using custom scripts written in MATLAB v15a with

252   the Machine Vision, Signal Processing and Fitting toolboxes (MathWorks, Natick MA USA); all

253   code is available on figshare at https://figshare.com/s/f8add694af9c79de7f76. Images stored as

254   jpeg files were calibrated and corrected for lens distortions using the MATLAB Camera

255   Calibration application, and then corrected for perspective distortions using MATLAB's

256   *fitgeotrans* and *imwarp* commands. Images captured using the UV and visible filters were

257   checked for alignment by hand and then converted into linearized and normalized measures of

258   reflectance, as explained under "Quantitative visual signal analysis" below.

259

260   To account for distance-dependent blurring due to each viewing species' visual acuity (Barnett et

261   al., 2018; Caves and Johnsen, 2018), multispectral images with linearized intensities were

262   spatially filtered before analysis to model the effect of viewing distance on contrasts between

263   feathers and background foliage, and its effect on contrasts within the patterned eyespot feathers

264   (See details in S3 Appendix). While peahens view peacock courtship displays at nearby distances

265   ≥ 1 to 2 m (Dakin and Montgomerie, 2009), we also modeled a variety of greater viewing

266   distances (2, 4, 8 and 16 m). Color patches were defined by hand in the original images and used

267   for each modeled distance for uniformity. After spatial filtering and before color and brightness

268   analysis, we sampled intensity values in the multispectral images on a square grid with spacing

269   equal to a visual acuity disk, following (Endler, 2012). To model the effect of spatial filtering on

270   the peacock's blue head, neck and breast plumage, we used an image with green foliage

271   background with an approximately peacock-shaped cutout of the blue plumage superimposed;

272   spatial filtering was performed using peacock body dimensions (Talha et al., 2018) to define the

273   composite image's effective spatial scale.

274

275   To approximate how the feathers appear in each viewer's visual system, three type of false color

276   images (ultraviolet, human visible RGB and viewer false color) were created from the

277   multispectral images in MATLAB using square-root transformed cone quantum catches, Q_{pr}

278   normalized to the maximum value of the brightest cone quantum catch on each image. To

279   represent the tetrachromatic vision of peafowl, an RGB image was created from the computed

280   LWS, MWS and SWS data, respectively and a magenta image was created using the VS cone

281   data.   To model dichromatic mammalian predator vision, we made up a single false color image

282   using blue to represent the S cone and yellow to represent the L cone quantum catch values.

283

Reflectance spectroscopy

285   We measured reflectance spectra using a model USB2000+ spectrometer and OceanView

286   software (Ocean Optics, Largo FL, USA) over the wavelength range 300–850 nm, using 100 ms

287   integration time, 3 pixel boxcar averaging (corresponding to the optical resolution of 6.5 pixels

288   = 2.06 nm FWHM), and averaging over 5 samples. All spectra were recorded in a dark room.

289   Samples were illuminated by an Ocean Optics PX-2 Pulsed Xenon Light source triggered at 200

290   Hz using square wave pulses from a model 330120A function generator (Agilent Technologies,

291   Wilmington, DE, USA); the source was turned on and allowed to warm up and stabilize for 15

292   minutes before data collection. Light for illumination and detection was carried in P400-1-UV-

293   VIS optical fibers transparent to 200 nm (Ocean Optics). We used two PTFE white standards

294   with flat 99.0% reflectance over 300-700 nm: a Spectralon USRS-99-010-EPV (Labsphere,

295   North Sutton, NH USA) and a model SM05CP2C (Thorlabs). White standard and dark currents

296   were measured every fifteen minutes. For each feather and each measurement geometry, raw

297   reflectance spectral data were recorded for each feather color patch sample radiance, AR, white

298   standard radiance, AR_r and dark current, D. The reflectance spectrum, $R(\lambda) = \frac{AR - D}{AR_r - D}$, was

299   smoothed over a wavelength interval of 20 nm using Savitzky-Golay smoothing in Origin; this

300   reduced high frequency noise but did not change reproducible features of the spectra peak

301   shapes.

302

303   Transmission spectra for the filters used in multispectral imaging were measured by recording

304   the spectrum of light reflected from the white standard with and without the filter inserted into

305   the light path with its face at normal incidence to the incident light. Reflectance values for color

306   and gray standards were measured using a RPH-SMA reflectance probe stand (Thorlabs, Newton

307   NJ USA) with the illuminating light at 45 deg to normal incidence and detected at normal

308   incidence. The reflectance goniometer for feather measurements used (S2 Fig) was adapted from

309   previously published designs (Van Wijk et al., 2016) (S2 Fig) but with an additional angular

310   degree of freedom to allow measurement of the bidirectional reflectance distribution function, in

311   which the angle of observation and illumination are not confined to the specular reflection

312   geometry (Vukusic and Stavenga, 2009). Both the illumination and detection optical pathways

313   were focused using a 74-UV lens (Ocean Optics) to a 2 mm diameter spot at about 5 cm from the

314   output surface of the lens. The feather samples were realigned every time the angle of

315   illumination and/or detection was adjusted to ensure both beams focused on the same region of

316   the feather. To assess reproducibility of spectra for the same color patch on each feather, we

317   measured each set of spectra three times for each sample after dismounting and remounting each

318   sample.

319

Quantitative visual signal analysis

321 We computed the color contrast, ΔS_c, between color patches in the feathers and background

322 vegetation in our multispectral images using the receptor noise limited color opponent model,

323 which has been shown to predict behavioral thresholds for visual signals in birds, humans and

324 insects (Vorobyev and Osorio, 1998). All calculations were performed using a custom

325 MATLAB script, which was tested by verifying that it computed the same values as the

326 multispectral analysis software package MICA version 1.22 (Troscianko and Stevens, 2015).

327 First, intensity values, V, from each multispectral image were corresponded to the actual

328 reflected irradiance, R, for this camera by an S-log transformation:

329
$$R(V) = Ae^{-\frac{V}{T_o}} + C. \tag{1}$$

330 The parameters A, T_o and C were obtained from nonlinear least squares fits in MATLAB

331 (adjusted-$R^2 \geq 0.997$) of the measured V and R values for each pixel in each RGB channel of the

332 image. The resulting fits then were used to convert measured intensity values for each pth color

333 patch into linearized and normalized reflected intensities (range [0,1]) for each combination of

334 filter and RGB image channel. To compute the color and brightness contrasts, these intensities

335 were converted into the cone quantum catch values, Q_{pr}, for each of the viewer's rth cone

336 photoreceptors:

337
$$Q_{pr} = \int I(\lambda) R_p(\lambda) S_r(\lambda) d\lambda / \int I(\lambda) S_r(\lambda) d\lambda, \tag{2}$$

338 where $I(\lambda)$ is the illumination spectrum, $S_r(\lambda)$ is the rth cone receptor's normalized spectral

339 sensitivity and $R_p(\lambda)$ is the pth patch's reflectance spectrum. Because birds and mammals are

340 known to achieve color constancy under a wide variety of illumination conditions (Kelber and

341 Osorio, 2010; Olsson et al., 2016), this equation also incorporates the von Kries transformation, a

342 mechanism for maintaining color constancy (Stoddard and Prum, 2008). To accomplish this

16

343   conversion, we used MICA to compute the parameters of a polynomial cone mapping between

344   the UV blue channel and the visible RGB channels of the multispectral images recorded by our

345   filter-camera system and the corresponding cone quantum catches, Q_{pr} (Stevens et al., 2007).

346   This software finds the optimal mapping using our measured filter transmission and camera RGB

347   spectral response curves with either the dichromatic ferret or tetrachromatic peafowl cone

348   spectral sensitivities, the CIE D65 illumination spectrum and a large database of natural spectra.

349   The net effect is to combine all measured values of linearized and normalized reflectance to

350   compute the quantum catch, Q_{pr}, of each rth cone (r = S or L for dichromats and r = VS, SWS,

351   MWS, or LWS for tetrachromats) for the pth sample color patch. Using a linear 2-way

352   interaction cone mapping model, we obtained a near perfect fit for each visual system: ferret (R^2

353   ≥ 0.999), peafowl ($R^2 \geq 0.996$) and blue tit (≥ 0.990 UVS cone, ≥ 0.998 all other cones).

354

355   The resulting cone quantum catch values, Q_{pr}, can be used to compute normalized color space

356   coordinates, for the $p t^{h}$ color patch: $q_p = \frac{Q_{pr}}{\Sigma_r Q_{pr}}$. For tetrachromats, the receptor index r = VS or

357   UVS, SWS, MWS, LWS and q_p = (v,s,m,l), while for dichromats r = S, L and q_p = (sw,lw).

358   After normalization, this corresponds to a three-dimensional tetrachromat color space for birds

359   and a one-dimensional colorspace for dichromats, here chosen to rely on sw. To validate the

360   results of our multispectral imaging code, we compared dichromat color space sw coordinates

361   computed by both MICA and our MATLAB code (sw_M) from our multispectral images with

362   those computed directly from reflectance spectra (sw_R) for six color chart squares. Use of the

363   camera and UV/visible filter cone mapping model was validated for multispectral image analysis

364   by the goodness of the linear fit, zero intercept and unit slope, between the two sets of color

365   space measures gave $sw_M = (0.018 \pm 0.031) + (1.00 \pm 0.07) \times sw_R +$ (adjusted-R^2 = 0.993) (S1

366   Fig).

367

368   To compute color contrasts, ΔS_c, we first computed the rth cone's log-linear quantum catch

369   (Weber-Fechner), $\log Q_{rp}$, for each pth patch. This was used to compute the difference in r^{th} cone

370   response for the pq^{th} patch pair, $\Delta_{rpq} = \log Q_{rp} - \log Q_{rq}$. The color contrast then is computed

371   from differences between opponent cone pairs weighted by receptor noise. Dichromats have only

372   S/L receptor opponency, so for them, $\Delta S_C = \left| \Delta_{Lpq} - \Delta_{Spq} \right| / \sqrt{e_L^2 + e_S^2}$ (Vorobyev and Osorio,

373   1998). The corresponding equation for color contrast in tetrachromats is more complicated

374   because all six possible combinations of the four single cones pairs should be considered

375   (Kelber, 2016):

376
$$\Delta S_C^2 = \frac{\begin{pmatrix} (e_S e_{VS})^2 (\Delta_L - \Delta_M)^2 + \left((e_M e_{VS})^2 (\Delta_L - \Delta_S)^2 \right) + \\ (e_S e_M)^2 (\Delta_L - \Delta_{VS})^2 + (e_S e_L)^2 (\Delta_M - \Delta_{VS})^2 + \\ (e_S e_M)^2 (\Delta_L - \Delta_{VS})^2 + (e_L e_M)^2 (\Delta_{VS} - \Delta_S)^2 \end{pmatrix}}{(e_S e_M e_L)^2 + (e_{VS} e_M e_L)^2 + (e_{VS} e_S e_L)^2 + (e_{VS} e_S e_M)^2} \tag{3}$$

377   For bright illumination levels, receptor noise is assumed to be a constant determined only by the

378   Weber fraction, w_f and the relative population density, g_r, for each rth cone class (Renoult et al.,

379   2015): $e_r = w_f / \sqrt{g_r}$. For peafowl, we used the value for chromatic Weber fractions of w_f =

380   0.06 for L cones for domestic chickens based on color discrimination (Olsson et al., 2015).

381   Receptor noise values for the other single cone classes were estimated using mean peafowl

382   relative population densities g_r = (0.477, 0.892, 1.047, 1) for (VS, SWS, MWS, LWS) (Hart,

383   2001), yielding e_r = (0.087, 0.064, 0.06, 0.06). For parrots, we used g_r = 0.25:0.33:1.05:1 and w_f

384   = 0.105 found for spectral sensitivity in *Melopsittacus undulatus* (Lind et al., 2014),

385   corresponding to e_r = (0.210, 0.182, 0.102, 0.105). Because color discrimination has not been

386   measured for other mammals (Olsson et al., 2017), following (Stoddard et al., 2019) we used w_f

387   = 0.22 found for brightness discrimination in domestic dogs (range 0.22-0.27) (Pretterer et al.,

388   2004). The relative cone population fractional densities measured for domestic cats (Linberg et

389   al., 2001) give a mean g_r(S,L) = (0.12,1); similar ratios have been reported for various wild felids

390   (Ahnelt et al., 2006) and domestic dogs (Mowat et al., 2008). This gives the estimated predator

391   receptor noise for color discrimination as (e_S, e_L) = (0.64, 0.22).

392

393   The brightness contrast, ΔS_L, between each pq[th] pair of color patches was computed from the

394   quantum catches, Q_{Lp} for the pth color patch for the spectral response for the luminance channel

395   (double cones for birds and L cones for dichromat predators) using ΔS_L = (log Q_{Lp} - log Q_{Lq})/w_f,

396   where w_f is the Weber fraction for brightness discrimination. For birds, we used w_f = 0.18

397   measured for double cones in budgerigars (*Melopsittacus undulatus*) (Lind et al., 2013); for

398   comparison, lower values 0.10 have been found for pigeons (Hodos et al., 1985) and higher

399   values ≥ 0.24 for chicks of the domestic chicken (Jones and Osorio, 2004). For predators, we

400   used w_f = 0.22 for brightness discrimination in domestic dogs as explained above; for

401   comparison, w_f = 0.10 in humans, and w_f ≤ 0.45 in other mammals (Maertens and Wichmann,

402   2013; Olsson et al., 2017).

403

404   Color and brightness contrasts are interpreted in units of just noticeable distances (JND), with

405   JND = 1 corresponding to the threshold for two patches to be discriminable under ideal

406   illumination and viewing conditions when suitable data exist for the visual system being

407   modeled (Olsson et al., 2015; Vorobyev and Osorio, 1998). Behavioral studies have shown that

408   birds detect colorful fruit at a rate that correlates with increasing color (but not brightness)

409   contrast for values >> 1 JND (Cazetta et al., 2009), while in lizards, the probability of

410   discriminating a color from its background was found to be < 20% at 1 JND and to scale

411   approximately linearly over the range $1 \leq JND \leq 12$ (Fleishman et al., 2016). Behavioral tests in

412   zebra finches have found that color contrast detection thresholds range from JND = 1 to 2.5 to

413   3.2, depending on background color (Lind, 2016). Following (Siddiqi et al., 2004), we therefore

414   assume that the contrast detection threshold is approximately JND = 1 and we define contrasts in

415   the range $1 < JND \leq 3$ as weakly detectable.

416

Pattern Analysis

418   To model the perception of visual texture of the peacock's train viewed against foliage, we also

419   performed granularity pattern analysis on the model peacock train photographs, using MATLAB

420   code adapted from (Barbosa et al., 2008) and MICA's granularity texture analysis package. In

421   granularity analysis, an image based on the luminance channel is filtered using an FFT bandpass

422   filter centered at a series of spatial frequencies (granularity bands). For each bandpass-filtered

423   image, the "pattern energy" (a measure of information at each spatial scale) is computed as the

424   standard deviation of its pixel intensity values. The "granularity spectrum" then is defined as

425   pattern energy vs granularity band. Granularity analysis was performed on the model peacock

426   train images processed for the dichromatic predator luminance channel as explained above.

427   Granularity spectra were computed for polygonal regions of interest (ROI) encompassing the

428   entire model train and each type of surrounding vegetation (i.e., tall grass, brush or trees). To

429   compensate for the effect of ROI shape and background, we used the following method adapted

430   from MICA. For each ROI, we first computed a masked image in which all regions outside the

431   ROI were replaced by a black background. Next, we created a mean masked image in which the

432   region inside the ROI in the masked image was replaced by the mean intensity within the ROI.

433   Identical granularity calculations were performed on both images and their difference was used

434   to create a shape-independent granularity spectrum.

435

436   We also computed summary statistics for comparing textures of the model train and its

437   background: total energy (the energy summed across all filter bands, which increases as pattern

438   contrast increases), peak filter size (the granularity band at peak energy; larger peak filter size

439   corresponds to smaller most prevalent feature size), and proportion energy (the maximum energy

440   divided by the total energy, a measure of how much of the spectral energy lies at the most

441   prevalent feature size; this decreases with increasing pattern scale diversity). Granularity

442   spectrum were plotted as "normalized energy" (pattern energy divided by total energy) vs

443   granularity band to give a measure of how pattern information is distributed across spatial scales.

444   Images with a uniform distribution of pattern scales have correspondingly uniform granularity

445   spectra, while images dominated by a single feature scale should have strongly peaked spectra.

446

447   Edge detection of the luminance channel image provides an alternative measure of pattern

448   complexity. We used the Canny edge filter in MATLAB to find edges using sigma = 3 and

449   threshold = 0.15 to 0.20 (relative to maximum luminance image intensity set to 1) (Lovell et al.,

450   2013; Melin et al., 2016). Model train images were first log transformed and then processed

451   using contrast-limited adaptive histogram equalization (Zuiderveld, 1994) (*adapthisteq* in

452   MATLAB) to detect texture edges in regions of widely differing illumination. The edge fraction

453   (percentage of edge pixels in each ROI) was then used to compare the model train with various

454   types of vegetation in the background (Stoddard et al., 2016); higher edge fractions indicate a

455   more complex pattern with more spatial features.

456

Statistics

458   Our analysis of color and brightness contrasts followed the two-step process recommended in

459   (Maia and White, 2018). First, to determine whether the mean color and brightness contrasts

460   between each patch pair had a statistically significant difference given their variances, we used

461   PERMANOVA modified for non-normal, heterogeneous data (Anderson et al., 2017)

462   implemented in the software package FATHOM (Jones, 2017) using 1000 bootstrap samples.

463   Note that is it possible for this difference to be statistically significant, but to have value too

464   small for it to be perceptually distinguishable. We therefore determined the effect size (how

465   perceptually distinct each color patch pair) as follows. We first drew with replacement 1000

466   bootstrapped sample pairs using the MATLAB command *datasample*, and computed the mean Δ

467   S_C and ΔS_L for this bootstrap resample. These mean contrasts were averaged over all images to

468   get the mean and s.e.m. for each color patch pair for each sample; the grand mean and s.e.m. then

469   was computed by averaging over all replicates for each feather type. Grand means and s.e.m. for

470   the texture summary statistics were calculated from the mean of each statistic taken over all

471   model train data for the train, grass, brush, and tree foliage. All results are reported as grand

472   mean [95% CI = 2 s.e.m].

473

Data Accessibility

475   All data and software required in order to replicate all of our results are archived either in the

476   supplemental materials or at https://figshare.com/s/f8add694af9c79de7f76.

477

Results

Reflectance spectroscopy

480 Reflectance spectra for peacock eyespot feather color patches (Fig 2D) and peacock iridescent

481 blue plumage (Fig. 2E) had spectral peaks consistent across repeated measured to 4 to 16 nm

482 (95% CI) and exhibited similar spectral peaks and overall shape to those measured for zero

483 elevation angle (Dakin and Montgomerie, 2013; Loyau et al., 2007; Yoshioka and Kinoshita,

484 2002). A comparison of cone spectral sensitivity data (Fig 2C) with these reflectance spectra

485 show that the peacock SWS cone is well matched to reflectance from its iridescent peacock blue

486 plumage. While the spectral peaks for the bronze (BZ), blue-green (BG) and outer loose green

487 (GB) barbs agree well with its SWS, MWS and LWS cone spectral ranges, all three also coincide

488 with the same L cone sensitivity for the predator. Both the predator and peafowl VS cone

489 spectral sensitivities also overlap with the reflectance spectrum from the eyespot's central BB

490 and PB dark violet patches. However, reflectance from these features is weak compared to the

491 other color patches, all of which also reflect weakly in the UV. Fig 2E shows the reflectance

492 spectrum of a representative green leaf, illustrating how its peak at approximately 550 nm and its

493 overall spectra resemble that of the peacock's loose green barbs; similar spectra for green

494 background foliage have been reported in (Cazetta, Schaefer, and Galetti 2009; Loyau et al.

495 2007).

496

497 Reflectance spectra for parrot feathers (Fig 3E) agreed with previously published values

498 (Tinbergen et al., 2013), confirming a good spectral match between yellow and red feather

499   reflectance with MWS and LWS avian cone sensitivities. The predator L cone sensitivity spans a

500   spectral range corresponding to longer wavelength reflection from both yellow and red pigments

501   (Fig. 3D). Both the yellow and red patches also have reflectance peaks in the UV with a better

502   overlap with bird UVS cone sensitivity than that of VS cones.

503

504   A comparison of the peak spectral sensitivities of S and L cones for canids, domestic cats and

505   ferrets with those for the four single cone populations of 21 bird species from 8 different orders

506   (Hart and Hunt, 2007) (Fig 5) illustrates that predator S cones have a peak response similar to

507   that of bird VS, but not UVS, cones. The predator S peak values lie between most peaks of the

508   avian UVS/VS and SWS cone populations, whereas predator M peak values lie between avian

509   MWS and LWS peak values.

510

511   **Fig 5. Comparison of peak spectral responses of predator and bird cones.** Peak single cone

512   spectral sensitivities for ferret S and L cones (Douglas & Jeffery, 2014) and for bird VS/UVS,

513   SWS,MWS and LWS cones from Fig 5B in (Hart & Hunt, 2007) for 21 species of birds from 9

514   orders.

515

516

517   ## Color and brightness contrast analysis

518   False color images and analyses using the receptor noise model of visual discrimination are

519   shown in Fig 6-9; all data and PERMANOVA pseudo-F and P values are reported in S1-S4

520   Datasets. Note that these false color images should be considered as a relative guide and not an

521   absolute indication of the detectability of contrasts because humans have better contrast

522   thresholds than dichromatic mammals by a factor of 3.7 for color and 2 for brightness, as well as

523   similar color contrast thresholds and better brightness thresholds by a factor of ≥ 1.6 for birds

524   (Olsson et al., 2015, 2017). To provide context for the measured color and brightness contrasts

525   between feathers and green saucer magnolia leaves, we also found that the contrasts between

526   leaves from the saucer magnolia and seven other plant species with different shades of green

527   were statistically significant (with one exception out of 27 pairs) with tetrachromatic bird vision

528    $\Delta S_C = 2.75$ [2.23, 3.28] and $\Delta S_L = 3.30$ [2.64, 3.97] and dichromatic mammal vision $\Delta S_C = 0.55$

529   [0.42, 0.69] and $\Delta S_L = 2.53$ [2.01, 3.06] (mean [95% CI]) (S3 Fig).

530

531   **Fig 6. False color images and color and brightness contrast analysis of peacock eyespot**

532   **feathers.** (A) False color images modelling peafowl and dichromatic mammalian predator

533   vision of peafowl eyespot and green leaf (inset at bottom of eyespot image) for different viewing

534   distances. Note that the false color images should be considered as a relative guide and not an

535   absolute indication of the detectability of contrasts because humans have better contrast

536   thresholds by a factor of 3.7 for color and 2 for brightness compared to dichromatic mammals.

537   (B)-(E) Estimated color (delta S_C) and brightness (delta S_L) contrasts for adjacent color patches

538   on the peacock eyespots and green vegetation, over a range of viewing distances. All data are

539   shown as grand means with 95% CI error bars. Contrasts corresponding to the same distance

540   have been displaced by horizontal jitter to avoid overlap. Data above the 1 JND line are above

541   the expected threshold for discrimination and contrasts within the grey shaded regions are at

542   most weakly detectable. Closed symbols indicate contrasts that are statistically significant in

543   each organism's colorspace (i.e., PERMANOVA $P < 0.05$); note that contrasts that are not

544 statistically significant (closed symbols) due to their large, overlapping variances in the

545 corresponding colorspace may still have mean values greater than the detection threshold.

546

547 **Fig 7. False color images and color and brightness contrast analysis of the peacock model**

548 **train photographed against various types of vegetation backgrounds.** (A) False color images

549 in peafowl and dichromatic mammalian predator vision of peafowl model train for different

550 viewing distances. (B)-(E) Color and luminance contrasts for the model train and features of

551 vegetation, over a range of viewing distances. All data are shown as grand means with 95% CI

552 error bars. See Fig 6 caption for further details.

553

554 **Fig 8. False color images and color and brightness contrast analysis of peacock blue neck**

555 **feathers used to model the body's appearance against green foliage.** (A) False color images

556 in peafowl and dichromatic mammalian predator vision of peacock blue breast plumage vs green

557 foliage for different viewing distances. (B)-(E) Color and luminance contrasts for the blue

558 plumage relative to green vegetation, over a range of viewing distances. See Fig 6 caption for

559 further details.

560

561 **Fig 9. False color images and color and brightness contrast analysis of parrot feathers.** (A)

562 False color images in parrot ultraviolet sensitive (UVS) and dichromatic mammalian predator

563 vision of scarlet macaw, African grey parrot and Amazon parrot red and yellow feathers vs green

564 leaf for different viewing distances. (B)-(E) Color and luminance contrasts for parrot feather

565 colors relative to green vegetation, over a range of viewing distances. See Fig 6 caption for

566 further details.

567

568   False color images for various simulated viewing distances are displayed for peacock eyespot

569   feathers in Fig 6A and visual signals are plotted vs distance in Fig 6B-E. In peafowl vision, all

570   pairs of adjacent color patches in the peacock's eyespot give large, statistically significant color

571   contrasts > 3 JND for all distances. The greatest color contrasts were between the blue-green

572   patch and surrounding rings and between the two central pupil-like patches; for some distances ≤

573   8 m these same pairs of color patches also had statistically significant brightness contrasts in the

574   1-3 JND low detectability range. By contrast, in dichromat vision none of the eyespot patch pairs

575   had color contrasts above 1 JND, and only the three innermost pairs of eyespot patches had

576   brightness contrasts that were in the weakly detectable 1-3 JND range.

577

578   For peafowl vision, at all distances the model peacock train had statistically significant color and

579   brightness contrasts that were > 3 JND for brush and trees, but not grass (Fig 7; additional false

580   color images in S4 Fig). In dichromat predator vision, all color contrasts for the model train were

581   < 1 JND and brightness contrasts were in the weakly detectable 1-3 JND range. Peacock blue

582   plumage was found to be perceptually detectable by conspecifics at all distances and to lie in the

583   weakly detectable 1-3 JND range for dichromat vision (Fig 8). The false color images of peacock

584   feathers (Fig 6, 7, 8, S4 Fig) demonstrate how color signals relative to background vegetation are

585   diminished when the single dichromat L cone replaces the separate SWS/MWS/LWS cones for

586   birds, especially at larger distances.

587

588   Red and yellow parrot feather color patches exhibited large, statistically significant contrasts in

589   avian UVS vision in general, with color contrasts > 3 JND for ≤ 8 m and brightness contrasts > 1

590   JND for most samples (Fig 9) By contrast, for dichromat vision, none of the red parrot patches

591   and the African grey parrot and scarlet macaw yellow patches had color contrasts > 1 JND, and

592   the Amazon parrot feather yellow patches just exceeded 1 JND for ≤ 4 m. For distances ≤ 8 m,

593   red parrot feather patches had brightness contrasts in the weakly detectable 1-3 JND range for ≤

594   8 m and yellow patches had mean values in the range 2.4-6.7 JND.

595

Pattern analysis

597   Fig 10 and S4 Fig show false color images and granularity spectra for the peacock's train and

598   different types of background vegetation (tall grass, brush and trees) for the various viewing

599   distances modeled (S5 Dataset). Because the spatial frequency of objects in an image as well as

600   an animal's visual field depend on distance, we would expect objects with similar textures

601   observed at different distances to have similarly-shaped spectra, but possibly different frequency

602   peaks and widths. Granularity spectra for the peacock's train (Fig. 10B) indeed had the same

603   shape as those for background vegetation in that each had a single broad peak for granularity

604   band values > 3. The peak spatial frequencies of each granularity spectrum moved to lower

605   values as viewing distance increased, as expected from the blurring of fine scale features. For all

606   distances, the peacock's train and background vegetation had values of proportion energy, peak

607   frequency and total energy that agreed at the 95% CI, with the only exception that the proportion

608   energy for distances > 4 m differed between the model train and trees (Fig. 9D-F). Collectively,

609   these results demonstrate that the peacock's erect train is an excellent match for the predominant

610   feature size distribution, overall contrast and pattern scale diversity of background vegetation.

611   Moreover, visual examination of the edge detected images (Fig 10A, S5 Fig) suggests that the

612   calculated edge fractions for the train and background foliage agreed at the 95% CI level at all

613   distances (Fig 9G).

614

615   **Fig 10. Texture analysis of the model peacock train photographed against various**

616   **vegetation backgrounds.** (A) Image based on dichromatic mammalian predator luminance

617   channel and (B) result of edge detection on the luminance image. (C) Granularity spectrum for

618   the model peacock train and three different regions of vegetation in the background vs viewing

619   distance. (D) Total spectral energy summed over the granularity spectrum, which gives a

620   measure of overall pattern contrast. (E) Proportional energy, a measure of how much the

621   dominant feature size dominates and hence pattern diversity; (F) spatial frequency at peak

622   spectral energy, which is inversely proportional to the predominant feature size; (G) edge

623   fraction, the proportion of the image corresponding to edges. Data are grand means for all model

624   train images and error bars show 95% CI.

625

Discussion

627   The results of our study show that sexually-selected color signals readily detectable by

628   conspecifics are not necessarily conspicuous to mammalian predators. Instead, for all distances

629   considered, the color and brightness contrasts for all feather samples studied here relative to

630   green foliage were much greater for birds than for dichromatic mammals. For viewing distances

631   of 1 m and more, most feather samples (peacock eyespot, model peacock train and red feathers,

632   and all yellow feathers but those of the scarlet macaw at ≤ 2 m) had color contrasts in

633   dichromatic vision that were perceptually indistinguishable from background vegetation at all

634   distances considered here. Unsurprisingly, the same feathers were highly conspicuous to

635   conspecifics: their color contrasts were comparable to values found for avian visual modeling for

636   fruit viewed against green foliage (Cazetta et al., 2009; Fadzly et al., 2013). The brightness

637   contrasts for these feathers vs background foliage in dichromatic predator vision were on the

638   whole greater than the corresponding color signals, although only values for yellow exceeded the

639   weakly detectable 1-3 JND range. This suggests that patterns with high brightness contrast, such

640   as those created by white and dark melanin-pigmented plumage, might be more readily

641   detectable by dichromat predators than color signals, and thus represent a greater detection risk

642   (Montgomerie et al., 2001). While the interpretation of supra-threshold color and brightness

643   contrasts is still debated (Stuart-Fox, 2018), our results show that such supranormal stimuli

644   remain detectable by conspecifics and other birds even at large distances where carnivores

645   cannot perceive them.

646

647   Considering parrot feathers in particular, we note that red plumage is at best weakly detectable

648   given its sub-threshold color contrasts and low brightness contrasts when viewed by dichromatic

649   mammals against green foliage, although yellow parrot feathers have brightness contrasts that

650   should be more readily detectable by mammalian predators at close distances. A consideration

651   of cone spectral sensitivities and feather reflectance spectra suggest two reasons for this

652   difference. First, these yellow feathers had an overall higher reflectance than the corresponding

653   red feathers, resulting in their having a higher brightness contrast relative to leaves. Second,

654   yellow feather pigments reflect considerable light in the UV compared to red pigments, whereas

655   UV reflectance is low for green plants. Yellow feathers thus stimulate both predator S and L

656   cones, while green plants primarily stimulate the L cones, providing a mechanism for

657   distinguishing yellow feathers from green foliage backgrounds.

658

659   These conclusions should hold for other birds with red and yellow plumage given that a wide

660   variety of species of birds have similar color vision to the species considered here (Fig 5), and

661   that feathers colored with carotenoid pigments have very similar reflectance spectra to the

662   pigment psittacofulvin found in parrot feathers (Shawkey and Hill, 2005; Toral et al., 2008).

663   Thus, our findings indicate that many species of red and yellow feathered birds that appear

664   conspicuous to other birds and humans may in fact be cryptic or poorly visible to predators

665   because of background matching (Stevens and Merilaita, 2011). Our findings also have broader

666   implications for interpreting how color cues, camouflage and possible eye mimicry appear to the

667   majority of mammals. Trichromacy in primates has been suggested to have evolved for a variety

668   of reasons (Carvalho et al., 2017), including detecting ripe fruit and immature leaves, breaking

669   camouflage (e.g., during foraging for eggs) (Troscianko et al., 2017), sexual or social signaling

670   (Hiramatsu et al., 2017), and predator detection (Pessoa et al., 2014). Our results suggest that the

671   evolution of trichromacy may also have provided catarryne primates, howler monkeys and some

672   marsupials with an advantage in detecting colorful birds, reptiles, amphibians and insects.

673

674   Ultraviolet vision per se does not result in these differing visual signals: these dichromatic

675   mammalian predators have similar near-UV S cone spectral sensitivity to the VS cones of birds

676   (Douglas and Jeffery, 2014; Stevens and Cuthill, 2007). Indeed, as noted above, since red and

677   yellow parrot feathers and the central patches on peacock feathers reflect appreciable UV light

678   this may make these feathers more detectable by dichromats. It is therefore important to include

679   UV reflectance in modeling of visual signals in dichromatic mammalian visual systems, as

680   opposed to relying on image processing of human visible RGB photographs (Pongrácz et al.

681   2017). These results also are not merely a consequence of birds having more types of cones than

682   carnivores: given the similar spectral response of dichromatic mammal S and L cones and avian

683   VS and MWS cones, color patches could in principle generate similar contrasts in both visual

684   systems. Instead, these feathers have low contrast in dichromatic mammal vision due to a

685   combination of low visual acuity, higher receptor noise levels and poorer spectral discrimination

686   over the L cone response range.

687

688   Focusing now on peacock eyespots, the large color contrasts for peafowl vision arise from

689   spectral tuning between the reflectance spectra of each peacock eyespot color patch and peafowl

690   single cone spectral sensitivities, similar to the agreement reported earlier between red and

691   yellow pigment reflectance spectra and tetrachromatic UVS cone responses for parrot plumage

692   and vision (Tinbergen et al., 2013). It is especially notable that the greatest color contrasts are

693   due to the blue-green ring, since its iridescence has been found to correlate with peacock mating

694   success (Dakin and Montgomerie, 2013; Loyau et al., 2007), and its chromatic contrast was

695   calculated to be the most salient signal in images of a displaying peacock (Pike, 2018).

696

697   When we computed measures for the model peacock train against a foliage background in

698   dichromatic predator vision, the train feathers were found to have below detection threshold

699   color contrasts and brightness contrasts in the low detectability 1-3 JND range, similar in

700   magnitude to those for various types of green vegetation. Taken together with the eyespot and

701   textural analysis results, this indicates that dichromatic mammalian predators are likely unable to

702   discriminate the peacock's train from green vegetation during foraging, although the eyespot's

703   innermost features create low detectable brightness contrasts at nearby distances. Contrary to

704   common assumption, this suggests the counterintuitive hypothesis that that both the color and

705   brightness contrasts might function as disruptive camouflage for peacocks viewed from a

706   distance, making the train difficult to distinguish as a whole (Hillgarth, 1984; Ridley et al., 1984;

707   Stevens and Merilaita, 2011).

708

709   The peacock's blue plumage had large, detectable levels of color contrast at all distances for

710   peafowl vision, though both color and brightness contrasts were in the low detectable range for

711   dichromatic predator vision. Thus, the blue head, neck and breast contour feathers may represent

712   a greater visual signal for distant conspecifics, as well as a greater predation risk, than the much

713   larger train; however, all of these values are likely less conspicuous when forest shade

714   diminishes their blue hue. Given that noniridescent blue feathers from other birds have been

715   shown to have similar reflectance spectra to peafowl blue plumage, these results are likely

716   generalizable (Osorio and Ham, 2002).

717

718   Do peacock eyespots mimic eyes in appearance when viewed by conspecifics or by predators?

719   Eyes and eye-like patterns have been shown to be highly salient visual signals for birds, humans

720   and domestic dogs (Somppi et al., 2016; Stevens and Ruxton, 2014; Yorzinski et al., 2015).

721   However, our false color images show that peafowl eyespots do not always appear to have a

722   central dark, circular pupil when viewed at typical display distances, either in peafowl or

723   dichromatic mammalian predator visual models (Fig 11A,B,C). Therefore, it is not obvious that

724   peacock ocelli appear eye-like to nearby viewers. On the other hand, blurring at larger distances

725   ≤ 8 m causes eyespots to appear to have pupil-like dark centers in dichromatic predator vision,

726   indicating that they may indeed appear eyelike to predators when viewed at this intermediate

727   range (Fig 11D).

728

729   **Fig. 11. False color images of peacock eyespots show that eye-mimicry depends on viewing**

730   **distance.** At 1 m, peacock eyespots have central features with brightness comparable to the

731   surrounding rings in false color images for peafowl vision in the (A) LWS/MWS/SWS and (B)

732   VS cone channels, and for dichromatic mammals (C). False color image of the model train in

733   dichromatic mammalian vision at 2 meters (D) show that the eyespots feature a darker pupil-like

734   center at distances ≤ 8 m.

735

736   Taken as a whole, these results call into question the widely-held assumption that the peacock's

737   eyespot feathers are highly conspicuous for all viewers. Indeed, (Hillgarth, 1984) noted that even

738   to humans the peacock's train can be well camouflaged against foliage in its native habitats and

739   (Ridley et al., 1984) has suggested that peafowl eyespots originated as a form of camouflage for

740   their native dappled light environments. Motion cues during peafowl displays and other

741   behaviors might enhance the detectability of their visual signals, although evidence is mixed

742   whether motion increases or decreases visual contrast thresholds (Hodos et al., 2003). On the

743   other hand, the motions of the flexible loose green barbs in the train might also simulate that of

744   background brush and grasses, a visual illusion studied in insects, crabs, spiders and lizards but

745   not yet in birds (Peters et al., 2008). Future video studies could utilize cameras adapted for

746   multispectral imaging provided with a filter that transmits light from the near-UV to 700 nm.

747

748   Supporting these conclusions, we have been unable to find any data in the literature supporting

749   the idea that the peacock with trains experience a significant, let alone an enhanced, risk of

750   predation compared to, e.g., either peacocks without trains or peahens. In fact, one survey of a

751   feral peafowl population (Petrie, 1992) found that predated adult peacocks tended to have

752   relatively small trains and lower mating success. Another study found that peafowl are preyed

753   on far less by leopards than expected given that they were the most abundant prey species in the

754   region studied (Mondal et al., 2011). Adult peacocks are reported to have several effective anti-

755   predator strategies, including running (Ali and Ripley, 1981; Thavarajah et al., 2016; Wilkinson

756   et al., 2015), flight (Askew, 2014), fighting with their sharp spurs (Petrie et al., 1991), hiding in

757   dense thickets (Ali and Ripley, 1981; Harikrishnan et al., 2010; de Silva et al., 1996), and using

758   group vigilance along with alarm calling (Yasmin and Yahya, 2000). At dusk, they roost in high

759   trees chosen for their protection against predators (de Silva et al., 1996; Trivedi and Johnsingh,

760   1996). As a result, peafowl appear to be at highest risk of predation primarily during their first

761   year (de Silva et al., 1996).

762

763   The available evidence thus indicates that any putative enhanced risk of predation or other

764   handicap suffered by adult peacocks is likely to be incurred by factors other than visual signals

765   created by their eyespot train feathers. For example, peacocks spend a large percentage of their

766   time maintaining their plumage (Walther, 2003) and displaying (Dakin and Montgomerie, 2009;

767   Harikrishnan et al., 2010). Thus, the elaborate courtship displays of peacocks may correspond to

768   handicaps due to the conspicuous appearance of their blue plumage, time lost from foraging for

769   food due to plumage maintenance and courtship displays, the male's likely inattention to

770   predators during displays, and the metabolic demands of the male's courtship displays

771   (Vehrencamp et al., 1989).

772

773   It is important to note that several other factors may result in feathers having even lower visual

774   contrasts in predator vision than reported here. First, our viewing and illumination geometries

775   were chosen to optimize color and brightness cues. Second, when feathers are viewed at low

776   illumination levels either in dim forest lighting or at twilight or night, they also are likely to have

777   lower color and brightness contrasts (Freitag and Pessoa, 2012; Sicsú et al., 2013). Furthermore,

778   since UV reflectance helps distinguish feathers from green foliage, the reduction in UV

779   irradiance in forest shade is likely to render feathers less detectable in forest shade than in direct

780   sunlight (Endler, 1993). Third, we also modeled only distance-dependent blurring due to visual

781   acuity (retinal sampling), but a more complete treatment would use each species' behaviorally

782   measured contrast sensitivity function (CSF) (Melin et al., 2016) to account for the optics of the

783   eye and other factors that have determined for our study species (Jarvis and Wathes, 2007).

784   While we lacked the data to perform this additional analysis, the additional blurring would make

785   dichromatic predators even less likely to be able to detect the feathers than our estimated

786   contrasts indicate. Fourth, we chose to compare feathers with relatively dark green leaves (S3

787   Fig). The small variation in color contrasts indicates our findings are generalizable to other

788   shades of green, while suggesting that feathers should be even less visible against light green

789   foliage. Thus, our results likely overestimate the detectability of these feathers by dichromatic

790   mammals.

791

792   The largest source of uncertainty in our analysis is the lack of behaviorally-measured Weber

793   fractions for color contrast for terrestrial carnivorans for the conditions considered here. This

794   data also would be valuable for studies that often have had to rely on human visual modeling in

795   analyzing egg camouflage (Stoddard et al., 2016) and the relationship between plumage,

796   brightness and antipredator vigilance (Pascual et al., 2014). The most relevant measures would

797   involve behavioral tests to determine whether these mammals can detect feathered model birds

798   when other cues (e.g., olfactory) are controlled for. Any such studies ought to be sure to use

799   illumination sources that include UV, as well as color cues that closely match the reflectance

800   spectra of natural objects (Stoddard et al., 2019).

801

802   Darwin stated that "Even the bright colors of many male birds cannot fail to make them

803   conspicuous to their enemies of all kinds" (Darwin, 1888). On the contrary, our study implies

804   that some species of birds that appear vividly colorful to humans and other birds may appear

805   drab and inconspicuous in the eyes of mammalian predators. This conclusion is consistent with

806   the finding that susceptibility to cat predation does not correlate significantly with sexual

807   dichromatism in birds (Møller et al., 2010). The predation risk incurred by colorful plumage

808   instead depends on specifics of pigmentation, photoreceptor response, and environmental

809   context, as suggested by sensory drive theory (Cummings and Endler, 2018), and thus should be

810   assessed on a case-by-case basis.

811

812   Predators have a variety of other means of detecting prey, including visual motion perception

813   and sensing acoustic, tactile and olfactory cues. Our results highlight the importance of

814   understanding how dynamic behaviors during multimodal displays, foraging and other activities

815 make birds more apparent to mammals and other predators than do their seemingly-conspicuous

816 colors alone.

Acknowledgements

818 We wish to thank Cassie Stoddard for providing us with her edge detection code, Charles Chubb

819 and Roger Hanlon for their granularity code, and Robert Beyer for instrumentation design.

820

Financial Disclosure

822 Haverford College awards to Suzanne Amador Kane, Rui Fang, and Yabin Lu, and Yuchao

823 Wang, www.haverford.edu; Natural Sciences and Engineering Research Council of Canada

824 (NSERC), Postdoctoral Fellowship to Roslyn Dakin www.nserc-crsng.gc.ca

825

Competing Interests

827 The authors have declared that no competing interests exist.

828

Author contributions

830 Conceptualization: S.A.K., R.D.; Methodology: S.A.K., R.F., Y.L., Y.W; Investigation: S.A.K,

831 R.F., Y.L., Y.W; Data curation: S.A.K., Y.W.; Software: S.A.K., Y.W.; Validation: S.A.K.,

832 Y.W.; Visualization: S.A.K., R.F., Y.L., Y.W; Formal analysis: S.A.K.,.W.; Writing – original

833 draft: S.A.K.; Writing – review & editing: S.A.K., R.D., R.F., Y.L., Y.W.

834 # References

835 Ahnelt, P.K., Schubert, C., Kübber-Heiss, A., Schiviz, A., and Anger, E. (2006). Independent
836 variation of retinal S and M cone photoreceptor topographies: A survey of four families of
837 mammals. Visual Neuroscience *23*, 429–435.

838 Akkaynak, D., Siemann, L.A., Barbosa, A., and Mäthger, L.M. (2017). Changeable camouflage:
839 how well can flounder resemble the colour and spatial scale of substrates in their natural
840 habitats? Royal Society Open Science *4*, 160824.

841 Ali, S., and Ripley, S.D. (1981). Handbook of the Birds of India and Pakistan: Together with
842 Those of Bangladesh, Nepal, Bhutan and Sri Lanka Volume 2: Megapodes to Crab Plover
843 (Oxford University Press).

844 Anderson, M.J., Walsh, D.C.I., Clarke, K.R., Gorley, R.N., and Guerra-Castro, E. (2017). Some
845 solutions to the multivariate Behrens–Fisher problem for dissimilarity-based analyses. Australian
846 & New Zealand Journal of Statistics *59*, 57–79.

847 Askew, G.N. (2014). The elaborate plumage in peacocks is not such a drag. Journal of
848 Experimental Biology *217*, 3237–3241.

849 Barbosa, A., Mäthger, L.M., Buresch, K.C., Kelly, J., Chubb, C., Chiao, C.-C., and Hanlon, R.T.
850 (2008). Cuttlefish camouflage: The effects of substrate contrast and size in evoking uniform,
851 mottle or disruptive body patterns. Vision Research *48*, 1242–1253.

852 Barnett, J.B., Michalis, C., Scott-Samuel, N.E., and Cuthill, I.C. (2018). Distance-dependent
853 defensive coloration in the poison frog Dendrobates tinctorius, Dendrobatidae. PNAS *115*,
854 6416–6421.

855 Barreira, A.S., García, N.C., Lougheed, S.C., and Tubaro, P.L. (2016). Viewing geometry affects
856 sexual dichromatism and conspicuousness of noniridescent plumage of Swallow Tanagers
857 (Tersina viridis). The Auk *133*, 530–543.

858 Beebe, W. (1918). A Monograph of the Pheasants (Witherby & Co).

859 Calderone, J.B., and Jacobs, G.H. (2003). Spectral properties and retinal distribution of ferret
860 cones. Visual Neuroscience *20*, 11–17.

861 Carvalho, L.S., Pessoa, D.M.A., Mountford, J.K., Davies, W.I.L., and Hunt, D.M. (2017). The
862 Genetic and Evolutionary Drives behind Primate Color Vision. Front. Ecol. Evol. *5*.

863 Caves, E.M., and Johnsen, S. (2018). AcuityView: An r package for portraying the effects of
864 visual acuity on scenes observed by an animal. Methods in Ecology and Evolution *9*, 793–797.

865 Cazetta, E., Schaefer, H.M., and Galetti, M. (2009). Why are fruits colorful? The relative
866 importance of achromatic and chromatic contrasts for detection by birds. Evol Ecol *23*, 233–244.

867 Chiao, C.-C., Wickiser, J.K., Allen, J.J., Genter, B., and Hanlon, R.T. (2011). Hyperspectral
868 imaging of cuttlefish camouflage indicates good color match in the eyes of fish predators. PNAS
869 *108*, 9148–9153.

870   Clark, D.L., and Clark, R.A. (2016). Neutral point testing of color vision in the domestic cat.
871   Experimental Eye Research *153*, 23–26.

872   Cronin, T.W., Johnsen, S., Marshall, N.J., and Warrant, E.J. (2014). Visual Ecology (Princeton
873   University Press).

874   Cummings, M.E., and Endler, J.A. (2018). 25 Years of sensory drive: the evidence and its
875   watery bias. Curr Zool *64*, 471–484.

876   Dakin, R., and Montgomerie, R. (2009). Peacocks orient their courtship displays towards the
877   sun. Behav Ecol Sociobiol *63*, 825–834.

878   Dakin, R., and Montgomerie, R. (2013). Eye for an eyespot: how iridescent plumage ocelli
879   influence peacock mating success. Behav Ecol *24*, 1048–1057.

880   Dakin, R., McCrossan, O., Hare, J.F., Montgomerie, R., and Kane, S.A. (2016). Biomechanics
881   of the peacock's display: How feather structure and resonance influence multimodal signaling.
882   PLOS ONE *11*, e0152759.

883   Dalrymple, R.L., Hui, F.K.C., Flores-Moreno, H., Kemp, D.J., and Moles, A.T. (2015). Roses are
884   red, violets are blue – so how much replication should you do? An assessment of variation in
885   the colour of flowers and birds. Biol J Linn Soc *114*, 69–81.

886   Darwin, C. (1888). The descent of man and selection in relation to sex (Murray).

887   Douglas, R.H., and Jeffery, G. (2014). The spectral transmission of ocular media suggests
888   ultraviolet sensitivity is widespread among mammals. Proceedings of the Royal Society of
889   London B: Biological Sciences *281*, 20132995.

890   Endler, J.A. (1980). Natural Selection on Color Patterns in Poecilia Reticulata. Evolution *34*, 76–
891   91.

892   Endler, J.A. (1991). Interactions between predator and prey. Behavioural Ecology 169–202.

893   Endler, J.A. (1993). The Color of Light in Forests and Its Implications. Ecological Monographs
894   *63*, 1–27.

895   Endler, J.A. (2012). A framework for analysing colour pattern geometry: adjacent colours. Biol J
896   Linn Soc *107*, 233–253.

897   Fadzly, N., Burns, K.C., and Zuharah, W.F. (2013). Evaluating Frugivore-fruit Interactions Using
898   Avian Eye Modelling. Trop Life Sci Res *24*, 31–50.

899   Fleishman, L.J., Perez, C.W., Yeo, A.I., Cummings, K.J., Dick, S., and Almonte, E. (2016).
900   Perceptual distance between colored stimuli in the lizard Anolis sagrei: comparing visual system
901   models to empirical results. Behav Ecol Sociobiol *70*, 541–555.

902   Freeman, A.R., and Hare, J.F. (2015). Infrasound in mating displays: a peacock's tale. Animal
903   Behaviour *102*, 241–250.

904   Freitag, F.B., and Pessoa, D.M.A. (2012). Effect of luminosity on color discrimination of
905   dichromatic marmosets (Callithrix jacchus). J. Opt. Soc. Am. A, JOSAA *29*, A216–A222.

906   Gokula, V. (2015). Display behaviour of Indian Peafowl Pavo cristatus (Aves: Galliformes)
907   during the mating season in viralimalai, TamilNadu, India. TAPROBANICA: The Journal of
908   Asian Biodiversity 7.

909   Guenther, E., and Zrenner, E. (1993). The spectral sensitivity of dark- and light-adapted cat
910   retinal ganglion cells. J. Neurosci. 13, 1543–1550.

911   Harikrishnan, S., Vasudevan, K., and Sivakumar, K. (2010). Behavior of Indian peafowl Pavo
912   cristatus Linn. 1758 during the mating period in a natural population. The Open Ornithology
913   Journal 3, 13–19.

914   Hart, N.S. (2001). Variations in cone photoreceptor abundance and the visual ecology of birds. J
915   Comp Physiol A 187, 685–697.

916   Hart, N.S. (2002). Vision in the peafowl (Aves: Pavo cristatus). Journal of Experimental Biology
917   205, 3925–3935.

918   Hart, N., and Hunt, D. (2007). Avian visual pigments: characteristics, spectral tuning, and
919   evolution. The American Naturalist 169, S7-26.

920   Hart, N.S., Partridge, J.C., Cuthill, I.C., and Bennett, A.T.D. (2000). Visual pigments, oil
921   droplets, ocular media and cone photoreceptor distribution in two species of passerine bird: the
922   blue tit (Parus caeruleus L.) and the blackbird (Turdus merula L.). J Comp Physiol A 186, 375–
923   387.

924   Håstad, O., Victorsson, J., and Ödeen, A. (2005). Differences in color vision make passerines
925   less conspicuous in the eyes of their predators. PNAS 102, 6391–6394.

926   Hillgarth, N. (1984). Social organization of wild peafowl in India. World Pheasant Assoc J 9, 47–
927   56.

928   Hiramatsu, C., Melin, A.D., Allen, W.L., Dubuc, C., and Higham, J.P. (2017). Experimental
929   evidence that primate trichromacy is well suited for detecting primate social colour signals. Proc.
930   R. Soc. B 284, 20162458.

931   Hodos, W., Bessette, B.B., Macko, K.A., and Weiss, S.R.B. (1985). Normative data for pigeon
932   vision. Vision Research 25, 1525–1527.

933   Hodos, W., Potocki, A., Ghim, M.M., and Gaffney, M. (2003). Temporal modulation of spatial
934   contrast vision in pigeons (Columba livia). Vision Research 43, 761–767.

935   Igoe, D., Parisi, A., and Carter, B. (2013). Characterization of a Smartphone Camera's
936   Response to Ultraviolet A Radiation. Photochemistry and Photobiology 89, 215–218.

937   Jacobs, G.H., Deegan, J.F., Crognale, M.A., and Fenwick, J.A. (1993). Photopigments of dogs
938   and foxes and their implications for canid vision. Visual Neuroscience 10, 173–180.

939   Jarvis, J.R., and Wathes, C.M. (2007). On the calculation of optical performance factors from
940   vertebrate spatial contrast sensitivity. Vision Research 47, 2259–2271.

941 Jensen, J.R. (2009). Remote sensing of the environment: An earth resource perspective 2/e
942 (Pearson Education India).

943 Jones, D.L. (2017). FATHOM: A Matlab toolbox for ecological and oceanographic data analysis
944 (St. Petersburg, FL USA: College of Marine Science, University of South Florida).

945 Jones, C.D., and Osorio, D. (2004). Discrimination of oriented visual textures by poultry chicks.
946 Vision Research *44*, 83–89.

947 Kasparson, A.A., Badridze, J., and Maximov, V.V. (2013). Colour cues proved to be more
948 informative for dogs than brightness. Proceedings of the Royal Society of London B: Biological
949 Sciences *280*, 20131356.

950 Kelber, A. (2016). Colour in the eye of the beholder: receptor sensitivities and neural circuits
951 underlying colour opponency and colour perception. Current Opinion in Neurobiology *41*, 106–
952 112.

953 Kelber, A., and Osorio, D. (2010). From spectral information to animal colour vision:
954 experiments and concepts. Proceedings of the Royal Society of London B: Biological Sciences
955 *277*, 1617–1625.

956 Linberg, K.A., Lewis, G.P., Shaaw, C., Rex, T.S., and Fisher, S.K. (2001). Distribution of S- and
957 M-cones in normal and experimentally detached cat retina. Journal of Comparative Neurology
958 *430*, 343–356.

959 Lind, O. (2016). Colour vision and background adaptation in a passerine bird, the zebra finch
960 (Taeniopygia guttata). Royal Society Open Science *3*, 160383.

961 Lind, O., Karlsson, S., and Kelber, A. (2013). Brightness Discrimination in Budgerigars
962 (Melopsittacus undulatus). PLOS ONE *8*, e54650.

963 Lind, O., Chavez, J., and Kelber, A. (2014). The contribution of single and double cones to
964 spectral sensitivity in budgerigars during changing light conditions. J Comp Physiol A *200*, 197–
965 207.

966 Loss, S., Will, T., and Marra, P. (2015). Direct mortality of birds from anthropogenic causes.
967 Annual Review of Ecology, Evolution, and Systematics *46*, 99–120.

968 Lovell, P.G., Ruxton, G.D., Langridge, K.V., and Spencer, K.A. (2013). Egg-Laying Substrate
969 Selection for Optimal Camouflage by Quail. Current Biology *23*, 260–264.

970 Loyau, A., Gomez, D., Moureau, B., Théry, M., Hart, N.S., Jalme, M.S., Bennett, A.T.D., and
971 Sorci, G. (2007). Iridescent structurally based coloration of eyespots correlates with mating
972 success in the peacock. Behav Ecol *18*, 1123–1131.

973 Maertens, M., and Wichmann, F.A. (2013). When luminance increment thresholds depend on
974 apparent lightness. Journal of Vision *13*, 21–21.

975 Maia, R., and White, T.E. (2018). Comparing colors using visual models. Behav Ecol *29*, 649–
976 659.

977 Melin, A.D., Kline, D.W., Hiramatsu, C., and Caro, T. (2016). Zebra Stripes through the Eyes of
978 Their Predators, Zebras, and Humans. PLOS ONE *11*, e0145679.

979 Miller, P.E., and Murphy, C.J. (1995). Vision in dogs. Journal-American Veterinary Medical
980 Association *207*, 1623–1634.

981 Møller, A.P., and Nielsen, J.T. (2006). Prey vulnerability in relation to sexual coloration of prey.
982 Behav Ecol Sociobiol *60*, 227–233.

983 Møller, A.P., Erritzøe, J., and Nielsen, J.T. (2010). Causes of interspecific variation in
984 susceptibility to cat predation on birds. Chinese Birds *1*, 97–111.

985 Mondal, K., Gupta, S., Qureshi, Q., and Sankar, K. (2011). Prey selection and food habits of
986 leopard (Panthera pardus fusca) in Sariska Tiger Reserve, Rajasthan, India. Mammalia *75*,
987 201–205.

988 Montgomerie, R., Lyon, B., and Holder, K. (2001). Dirty ptarmigan: behavioral modification of
989 conspicuous male plumage. Behav Ecol *12*, 429–438.

990 Mowat, F.M., Petersen-Jones, S.M., Williamson, H., Williams, D.L., Luthert, P.J., Ali, R.R., and
991 Bainbridge, J.W. (2008). Topographical characterization of cone photoreceptors and the area
992 centralis of the canine retina. Mol Vis *14*, 2518–2527.

993 Neitz, J., Geist, T., and Jacobs, G.H. (1989). Color vision in the dog. Visual Neuroscience *3*,
994 119–125.

995 Nokelainen, O., Hubbard, N., Lown, A.E., Wood, L.E., and Stevens, M. (2017). Through
996 predators' eyes: phenotype–environment associations in shore crab coloration at different
997 spatial scales. Biol J Linn Soc *122*, 738–751.

998 Olsson, P., Lind, O., and Kelber, A. (2015). Bird colour vision: behavioural thresholds reveal
999 receptor noise. Journal of Experimental Biology *218*, 184–193.

1000 Olsson, P., Wilby, D., and Kelber, A. (2016). Quantitative studies of animal colour constancy:
1001 using the chicken as model. Proc. R. Soc. B *283*, 20160411.

1002 Olsson, P., Lind, O., and Kelber, A. (2017). Chromatic and achromatic vision: parameter choice
1003 and limitations for reliable model predictions. Behav Ecol *29*, 273–282.

1004 Osorio, D., and Ham, A.D. (2002). Spectral reflectance and directional properties of structural
1005 coloration in bird plumage. Journal of Experimental Biology *205*, 2017–2027.

1006 Osorio, D., and Vorobyev, M. (2005). Photoreceptor spectral sensitivities in terrestrial animals:
1007 adaptations for luminance and colour vision. Proceedings of the Royal Society of London B:
1008 Biological Sciences *272*, 1745–1752.

1009 Outomuro, D., Söderquist, L., Johansson, F., Ödeen, A., and Nordström, K. (2017). The price of
1010 looking sexy: visual ecology of a three-level predator–prey system. Functional Ecology *31*, 707–
1011 718.

43

1012 Pascual, J., Senar, J.C., and Domènech, J. (2014). Plumage brightness, vigilance, escape
1013 potential, and predation risk in male and female Eurasian Siskins (Spinus spinus). The Auk *131*,
1014 61–72.

1015 Pessoa, D.M.A., Maia, R., Ajuz, R.C. de A., Moraes, P.Z.P.M.R.D., Spyrides, M.H.C., and
1016 Pessoa, V.F. (2014). The adaptive value of primate color vision for predator detection. American
1017 Journal of Primatology *76*, 721–729.

1018 Peters, R., Hemmi, J., and Zeil, J. (2008). Image motion environments: background noise for
1019 movement-based animal signals. J Comp Physiol A *194*, 441–456.

1020 Petrie, M. (1992). Peacocks with low mating success are more likely to suffer predation. Animal
1021 Behaviour *44*, 585–586.

1022 Petrie, M., Tim, H., and Carolyn, S. (1991). Peahens prefer peacocks with elaborate trains.
1023 Animal Behaviour *41*, 323–331.

1024 Pike, T.W. (2018). Quantifying camouflage and conspicuousness using visual salience.
1025 Methods in Ecology and Evolution *9*, 1883–1895.

1026 Pretterer, G., Bubna-Littitz, H., Windischbauer, G., Gabler, C., and Griebel, U. (2004).
1027 Brightness discrimination in the dog. Journal of Vision *4*, 10–10.

1028 Prutchi, D. (2016). Exploring Ultraviolet Photography (Amherst Media).

1029 Ranjith, V., and Jose, B. (2016). Habitat preference of Indian peafowl (Pavo cristatus) in
1030 selected areas of Palakkad district, Kerala, India. Current Science *110*, 2177–2182.

1031 Renoult, J.P., Kelber, A., and Schaefer, H.M. (2015). Colour spaces in ecology and evolutionary
1032 biology. Biological Reviews *92*, 292–315.

1033 Ridley, M.W., Lelliott, A.D., and Rands, M.R.W. (1984). The courtship display of feral peafowl.
1034 Journal of World Pheasant Association *9*, 57–68.

1035 Robbins, C.S. (1981). Effect of time of day on bird activity. Studies in Avian Biology *6*, 275–286.

1036 Ruxton, G.D., Sherratt, T.N., and Speed, M.P. (2004). Avoiding Attack: The Evolutionary
1037 Ecology of Crypsis, Warning Signals and Mimicry (OUP Oxford).

1038 Sharma, I.K. (1974). Ecological Studies of the Plumes of the Peacock (Pavo cristatus). The
1039 Condor *76*, 344–346.

1040 Shawkey, M.D., and Hill, G.E. (2005). Carotenoids need structural colours to shine. Biology
1041 Letters *1*, 121–124.

1042 Sicsú, P., Manica, L.T., Maia, R., and Macedo, R.H. (2013). Here comes the sun: multimodal
1043 displays are associated with sunlight incidence. Behav Ecol Sociobiol *67*, 1633–1642.

1044 Siddiqi, A., Cronin, T.W., Loew, E.R., Vorobyev, M., and Summers, K. (2004). Interspecific and
1045 intraspecific views of color signals in the strawberry poison frog Dendrobates pumilio. Journal of
1046 Experimental Biology *207*, 2471–2485.

1047 de Silva, P.K., Santiapillai, C., and Dissanayake, S. (1996). Some aspects of the population
1048 ecology of the blue peafowl, Pavo cristatus, in Ruhuna National Park, Sri Lanka. Journal of
1049 South Asian Natural History *2*, 113–126.

1050 Somppi, S., Törnqvist, H., Kujala, M.V., Hänninen, L., Krause, C.M., and Vainio, O. (2016).
1051 Dogs Evaluate Threatening Facial Expressions by Their Biological Validity – Evidence from
1052 Gazing Patterns. PLOS ONE *11*, e0143047.

1053 Spitschan, M., Aguirre, G.K., Brainard, D.H., and Sweeney, A.M. (2016). Variation of outdoor
1054 illumination as a function of solar elevation and light pollution. Scientific Reports *6*, 26756.

1055 Stevens, M., and Cuthill, I.C. (2007). Hidden Messages: Are Ultraviolet Signals a Special
1056 Channel in Avian Communication? BioScience *57*, 501–507.

1057 Stevens, M., and Merilaita, S. (2011). Animal Camouflage: Mechanisms and Function
1058 (Cambridge University Press).

1059 Stevens, M., and Ruxton, G.D. (2014). Do animal eyespots really mimic eyes? Current Zoology
1060 *60*, 26–36.

1061 Stevens, M., Párraga, C.A., Cuthill, I.C., Partridge, J.C., and Troscianko, T.S. (2007). Using
1062 digital photography to study animal coloration. Biol J Linn Soc *90*, 211–237.

1063 Stoddard, M.C., and Prum, R.O. (2008). Evolution of Avian Plumage Color in a Tetrahedral
1064 Color Space: A Phylogenetic Analysis of New World Buntings. The American Naturalist *171*,
1065 755–776.

1066 Stoddard, M.C., and Stevens, M. (2010). Pattern mimicry of host eggs by the common cuckoo,
1067 as seen through a bird's eye. Proceedings of the Royal Society of London B: Biological
1068 Sciences rspb20092018.

1069 Stoddard, M.C., Kupán, K., Eyster, H.N., Rojas-Abreu, W., Cruz-López, M., Serrano-Meneses,
1070 M.A., and Küpper, C. (2016). Camouflage and Clutch Survival in Plovers and Terns. Scientific
1071 Reports *6*, 32059.

1072 Stoddard, M.C., Miller, A.E., Eyster, H.N., and Akkaynak, D. (2019). I see your false colours:
1073 how artificial stimuli appear to different animal viewers. Interface Focus *9*, 20180053.

1074 Stuart-Fox, D. (2018). Opening the "black box" of modeling animal color vision: a comment on
1075 Olsson et al. Behav Ecol *29*, 284–284.

1076 Sumner, P., and Mollon, J.D. (2003). Colors of primate pelage and skin: Objective assessment
1077 of conspicuousness. American Journal of Primatology *59*, 67–91.

1078 Talha, M.M.H., Mia, M.M., and Momu, J.M. (2018). Morphometric, productive and reproductive
1079 traits of Indian peafowl (Pavo cristatus) in Bangladesh. International Journal of Development
1080 Research *8*, 19039–19043.

1081 Thavarajah, N.K., Tickle, P.G., Nudds, R.L., and Codd, J.R. (2016). The peacock train does not
1082 handicap cursorial locomotor performance. Scientific Reports *6*, 36512.

45

1083   Théry, M., Debut, M., Gomez, D., and Casas, J. (2005). Specific color sensitivities of prey and
1084   predator explain camouflage in different visual systems. Behav Ecol *16*, 25–29.

1085   Tinbergen, J., Wilts, B.D., and Stavenga, D.G. (2013). Spectral tuning of Amazon parrot feather
1086   coloration by psittacofulvin pigments and spongy structures. Journal of Experimental Biology
1087   jeb.091561.

1088   Toral, G.M., Figuerola, J., and Negro, J.J. (2008). Multiple ways to become red: Pigment
1089   identification in red feathers using spectrometry. Comparative Biochemistry and Physiology Part
1090   B: Biochemistry and Molecular Biology *150*, 147–152.

1091   Trivedi, P., and Johnsingh, A.J.T. (1996). Roost selection by Indian Peafowl (Pavo cristatus) in
1092   Gir Forest, India. Journal of the Bombay Natural Histroy Society *93*, 25–29.

1093   Troscianko, J., and Stevens, M. (2015). Image calibration and analysis toolbox – a free software
1094   suite for objectively measuring reflectance, colour and pattern. Methods in Ecology and
1095   Evolution *6*, 1320–1331.

1096   Troscianko, J., Wilson-Aggarwal, J., Griffiths, D., Spottiswoode, C.N., and Stevens, M. (2017).
1097   Relative advantages of dichromatic and trichromatic color vision in camouflage breaking. Behav
1098   Ecol *28*, 556–564.

1099   Van Wijk, S., Bélisle, M., Garant, D., and Pelletier, F. (2016). A reliable technique to quantify the
1100   individual variability of iridescent coloration in birds. Journal of Avian Biology *47*, 227–234.

1101   Vehrencamp, S.L., Bradbury, J.W., and Gibson, R.M. (1989). The energetic cost of display in
1102   male sage grouse. Animal Behaviour *38*, 885–896.

1103   Vogt, M.C., and Vogt, M.E. (2016). RESEARCH ARTICLE: Near-Remote Sensing of Water
1104   Turbidity Using Small Unmanned Aircraft Systems. Environmental Practice *18*, 18–31.

1105   Vorobyev, M., and Osorio, D. (1998). Receptor noise as a determinant of colour thresholds.
1106   Proceedings of the Royal Society of London B: Biological Sciences *265*, 351–358.

1107   Vukusic, P., and Stavenga, D.G. (2009). Physical methods for investigating structural colours in
1108   biological systems. Journal of The Royal Society Interface *6*, S133–S148.

1109   Walther, B.A. (2003). Do peacocks devote maintenance time to their ornamental plumage?
1110   Time budgets of male blue peafowl Pavo cristatus. Lundiana *4*, 149–154.

1111   Wilkinson, H., Thavarajah, N., and Codd, J. (2015). The metabolic cost of walking on an incline
1112   in the Peacock (Pavo cristatus). PeerJ *3*, e987.

1113   Yasmin, S., and Yahya, H.S.A. (2000). Group size and vigilance in Indian peafowl. Journal of
1114   the Bombay Natural History Society *97*, 425–428.

1115   Yorzinski, J.L., Patricelli, G.L., Babcock, J.S., Pearson, J.M., and Platt, M.L. (2013). Through
1116   their eyes: selective attention in peahens during courtship. Journal of Experimental Biology *216*,
1117   3035–3046.

46

1118   Yorzinski, J.L., Platt, M.L., and Adams, G.K. (2015). Eye-spots in Lepidoptera attract attention in
1119   humans. R Soc Open Sci *2*.

1120   Yoshioka, S., and Kinoshita, S. (2002). Effect of macroscopic structure in iridescent color of the
1121   peacock feathers. Forma-Tokyo *17*, 169–181.

1122   Yun, H.S., Park, S.H., Kim, H.-J., Lee, W.D., Lee, K.D., Hong, S.Y., and Jung, G.H. (2016). Use
1123   of Unmanned Aerial Vehicle for Multi-temporal Monitoring of Soybean Vegetation Fraction.
1124   Journal of Biosystems Engineering *41*, 126–137.

1125   Zahavi, A. (1975). Mate selection—A selection for a handicap. Journal of Theoretical Biology
1126   *53*, 205–214.

1127   Zuiderveld, K. (1994). Contrast Limited Adaptive Histogram Equalization. Graphics Gems 474–
1128   485.

Supporting information captions

1129

1130   **S1 Appendix. Predators of Indian peafowl.**

1131

1132

1133   **S2 Appendix. Species of plants used for background foliage in multispectral images.**

1134

1135

1136   **S3 Appendix. Methods for spatially filtering multispectral images to account for visual**

1137   **acuity effects at varying viewing distances.**

1138

1139   **S1 Fig. Multispectral camera specifications: image sensor spectral response and filter**

1140   **transmission spectra.**

1141

1142   **S2 Fig. Reflectance spectroscopy apparatus and multispectral camera filming setup.**

1143

1144   **S3 Fig. Various green leaves imaged and analyzed for comparison with feather samples**

1145   **and the saucer magnolia leaves used as a background.**

1146

47

1147 **S4 Fig. Model train false color images.**

1148

1149 **S5 Fig. Model peacock train edge detected images.**

1150

1151

1152 **S1 Dataset. Color and brightness contrast data and PERMANOVA pseudo-F and P values**

1153 **for Indian peacock eyespot feathers**

1154

1155 **S2 Dataset. Color and brightness contrast data and PERMANOVA pseudo-F and P values**

1156 **for model Indian peacock train**

1157

1158 **S3 Dataset. Color and brightness contrast data and PERMANOVA pseudo-F and P values**

1159 **for Indian peacock blue body feathers**

1160

1161 **S4 Dataset. Color and brightness contrast data and PERMANOVA pseudo-F and P values**

1162 **for parrot feathers**

1163

1164 **S5 Dataset. Granularity and edge-detection visual texture data for model Indian peacock**

1165 **train**

1166

1167

1168

1169

A

Scarlet macaw
SWS/MWS/LWS
false color

Scarlet macaw
UVS
false color

Dichromat
predator
false color

African grey parrot
SWS/MWS/LWS
false color

African grey parrot
UVS
false color

Dichromat
predator
false color

Amazon parrot
SWS/MWS/LWS
false color

Amazon parrot
UVS
false color
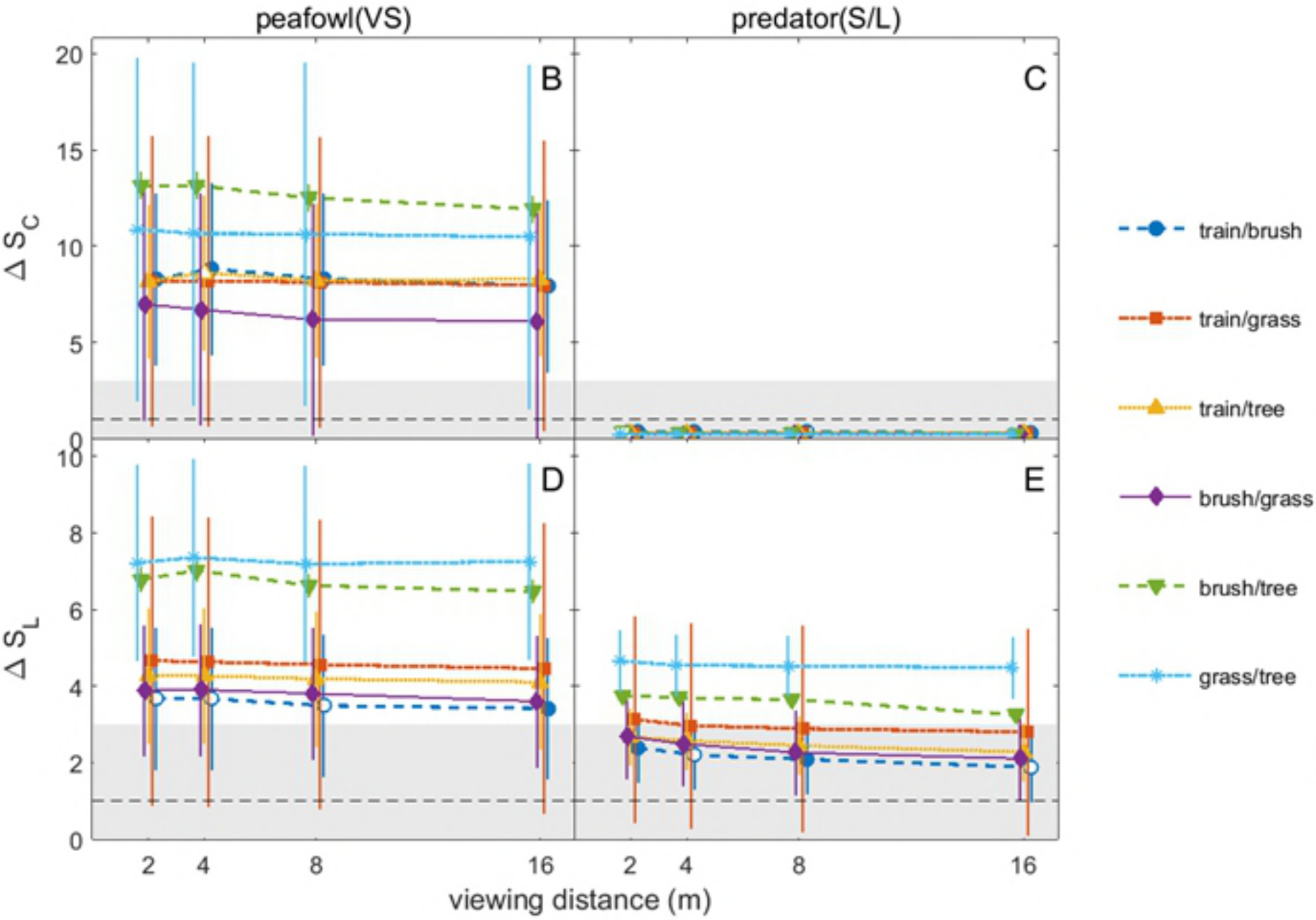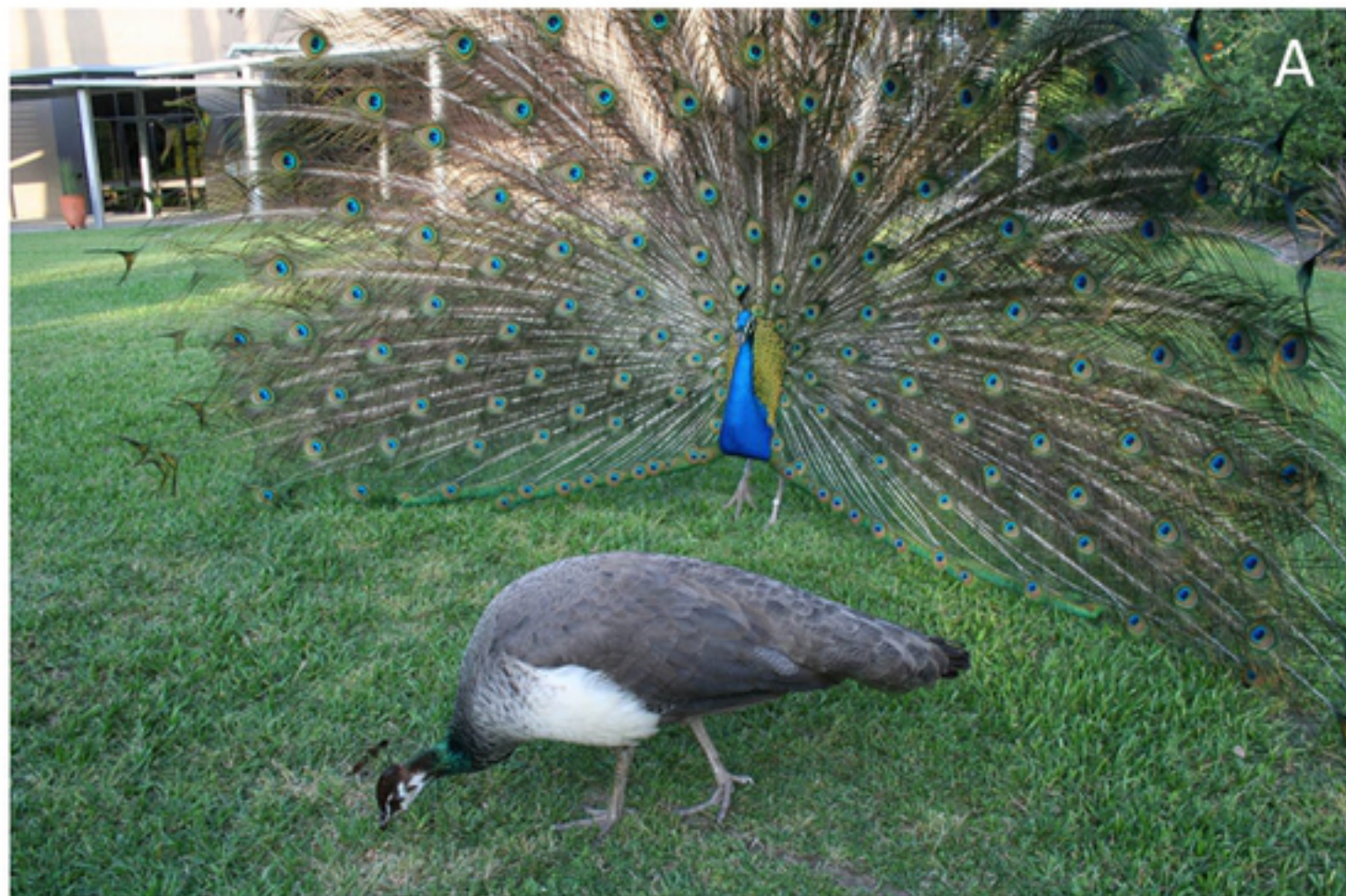
Dichromat
predator
false color

1 m   2 m   4 m   8 m   16 m

parrot (UVS)   predator (S/L)

B   C

ΔS_C

D   E

ΔS_L

viewing distance (m)

- - ● - - African grey parrot red
——■—— Amazon parrot red
——▲—— Amazon parrot yellow
- - ◆ - - scarlet macaw red
——▼—— scarlet macaw yellow

< detection threshold
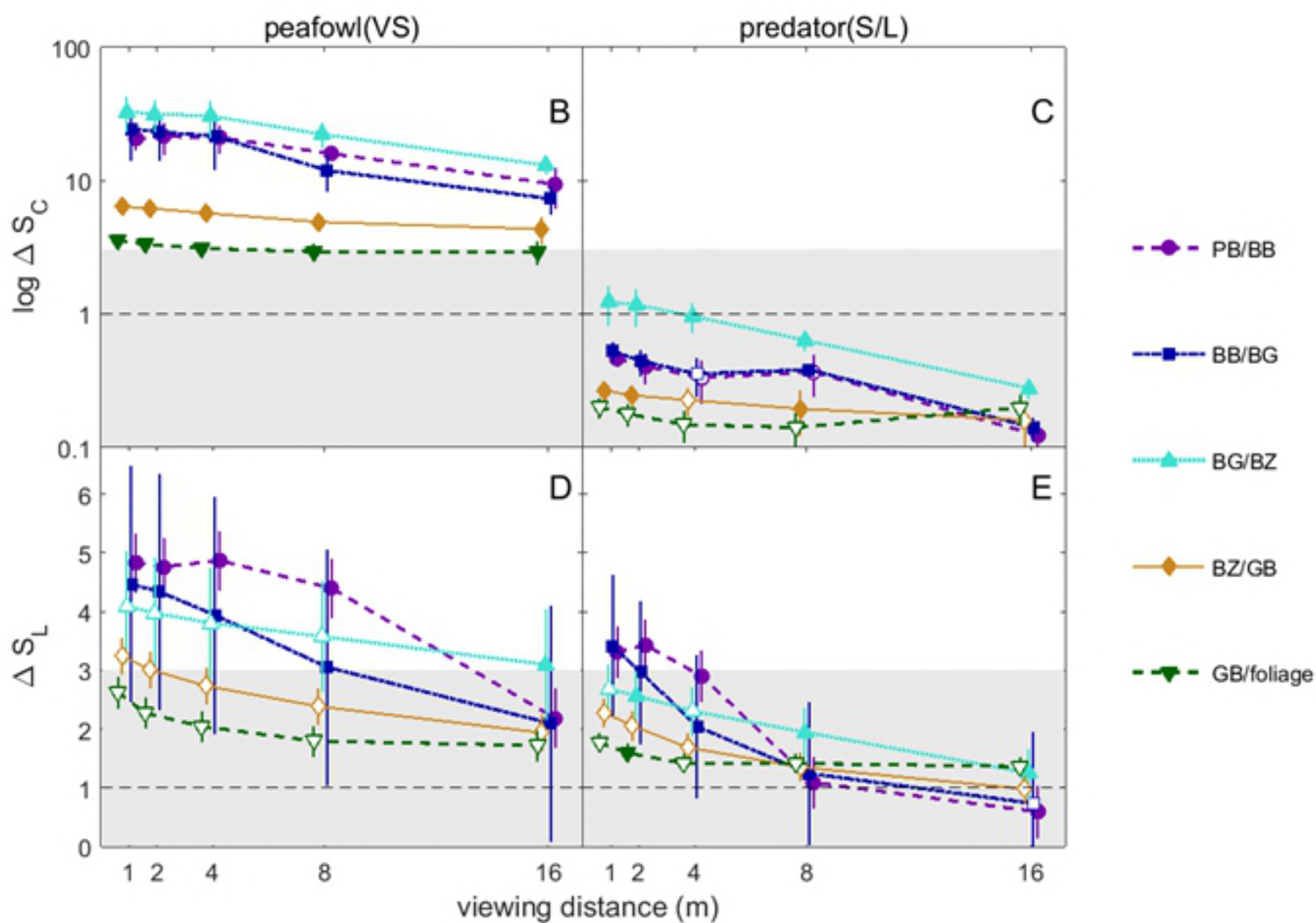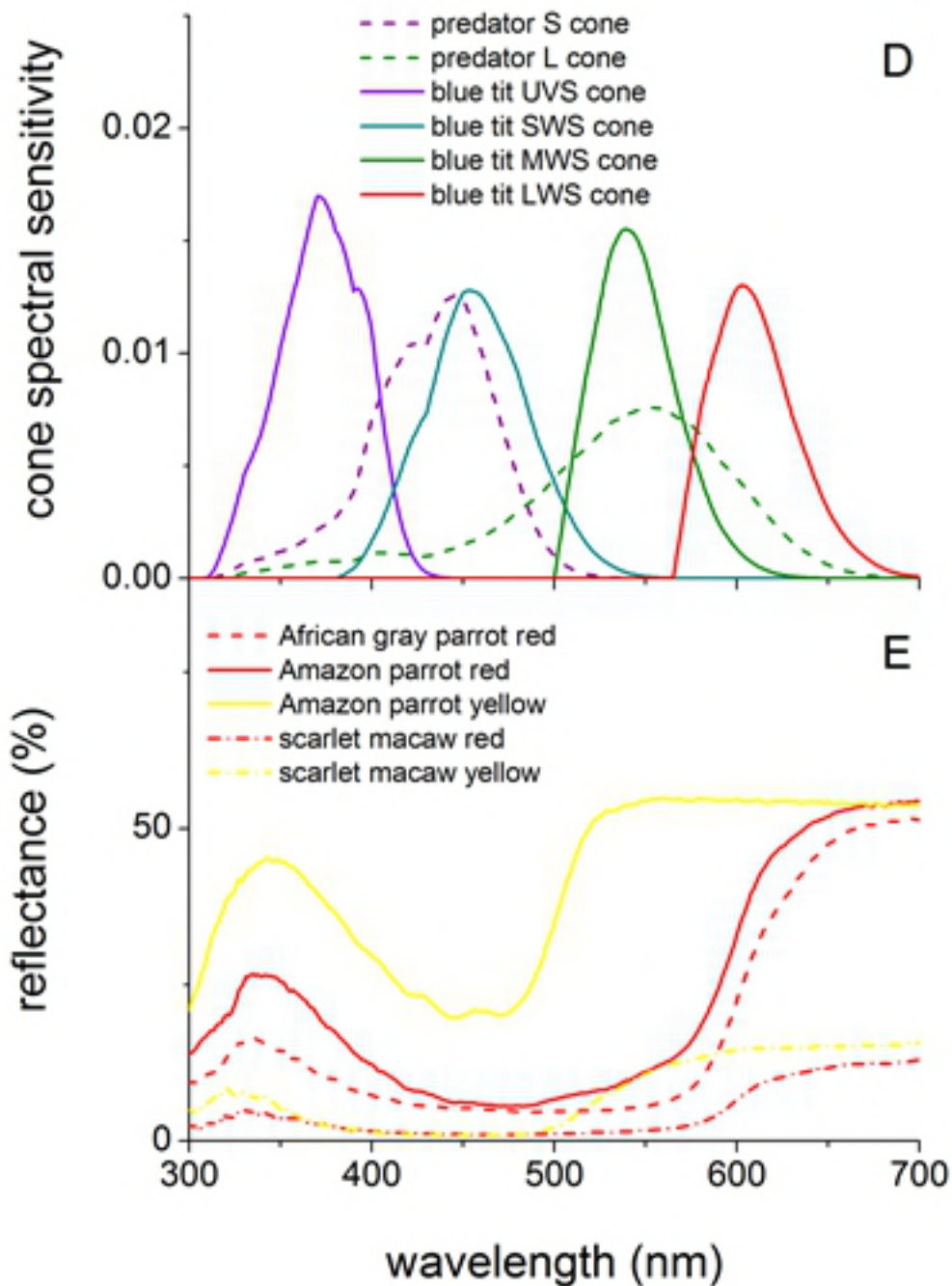
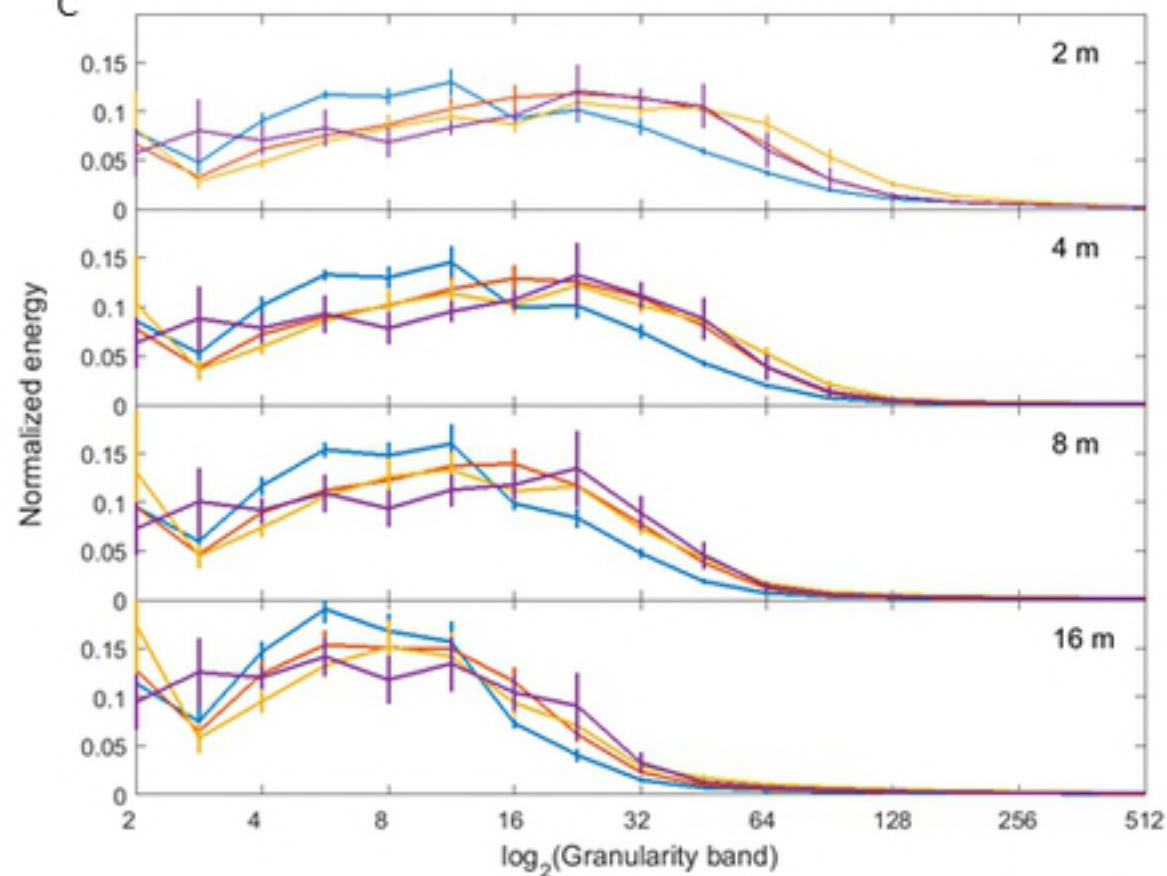A — Predator luminance (2 m)

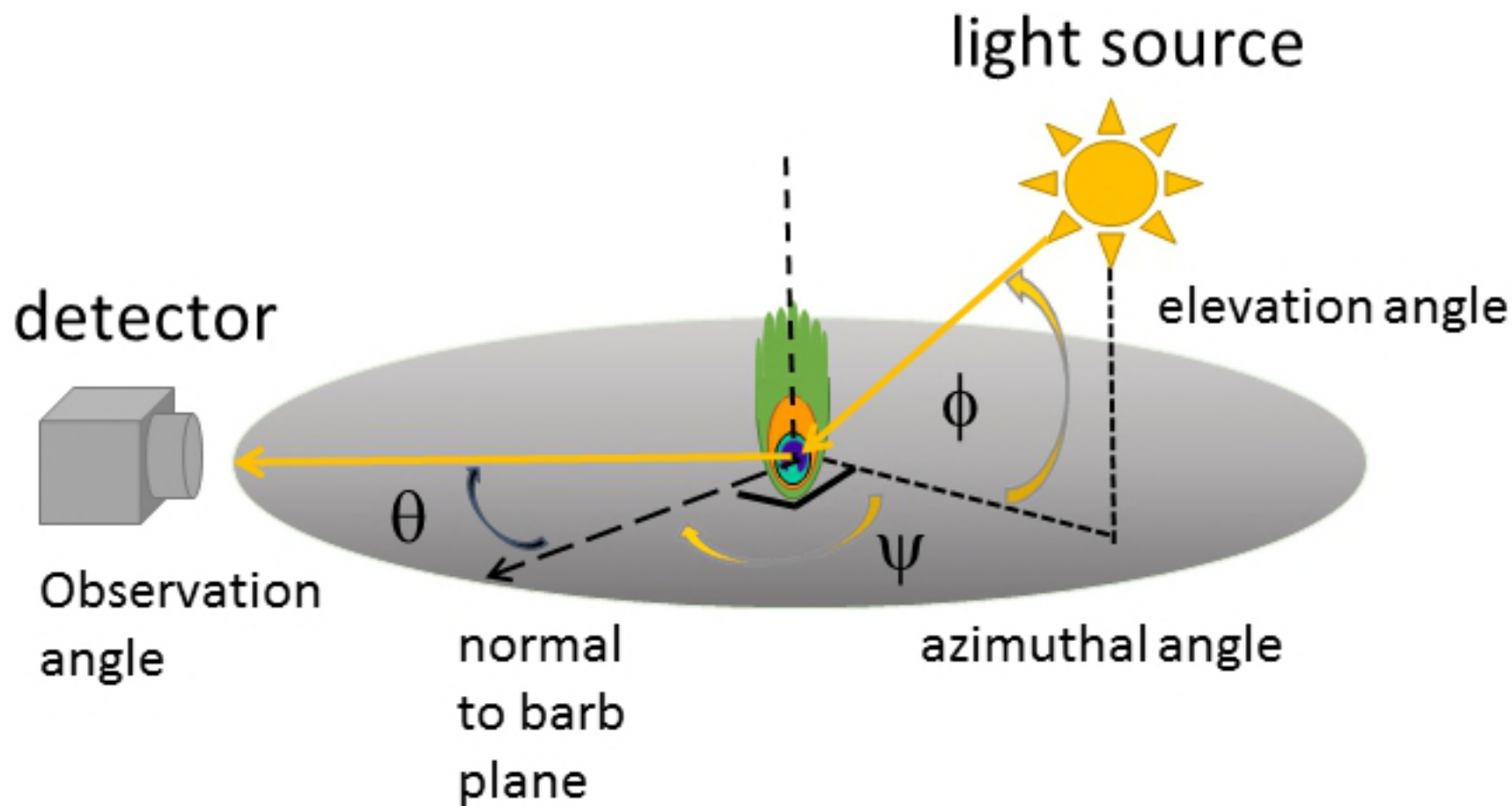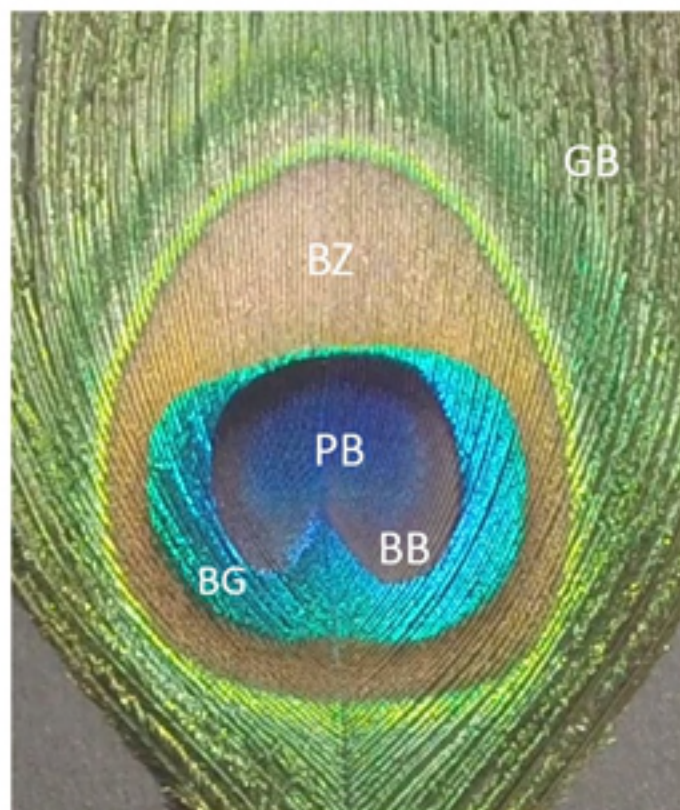B — Edge detection based on predator luminance (2 m)

C

Normalized energy vs log₂(Granularity band), at 2 m, 4 m, 8 m, 16 m

Legend: train, brush, grass, tree

D — total energy — increasing / overall pattern contrast / decreasing

E — proportion energy — decreasing / pattern diversity / increasing

F — peak filter size — increasing / predominant feature size / decreasing

G — edge fraction — increasing / percent edges / decreasing

viewing distance (m)

light source

detector

elevation angle

ϕ

θ

Observation
angle

ψ

normal
to barb
plane

azimuthal angle

A

GB

BZ

PB

BB

BG

B

C

predator S
predator L
peafowl VS
peafowl SWS
peafowl MWS
peafowl LWS

cone spectral sensitivity

0.02

0.01

0.00

D

Purple Black (PB)
Blue Black (BB)
Blue Green (BG)
Bronze-gold (BZ)
Green Barbule (GB)

reflectance (%)

20

10

0

E

green leaf
blue peacock feather

reflectance (%)

20

10

0

300   400   500   600   700

wavelength (nm)